Acta Neuropathologica (2025) 150:51
https://doi.org/10.1007/s00401-025-02956-6

ORIGINAL PAPER

The G2019S LRRK2 mutation exacerbates α-synuclein and tau neuropathology through divergent pathways in Parkinson's disease models

George Tsafaras[1,2,4] · Diego Cabezudo[1,3] · Lot Wetzels[1] · Iraklis Tsakogias[1] · Ajantha Abey[2,4] · Eduard Bentea[1] · Maria Sanchiz-Calvo[1] · Chris Van den Haute[1,5] · Richard Wade-Martins[2,4] · Veerle Baekelandt[1]

Received: 18 July 2025 / Revised: 29 October 2025 / Accepted: 30 October 2025

Abstract

Aggregated α-synuclein (αSyn) is a pathological hallmark of Parkinson's disease (PD), yet other protein aggregates, including tau, are commonly observed in PD brains. This suggests that PD is not solely a synucleinopathy but may involve multiple, coexisting proteinopathies. Mutations in LRRK2, particularly the G2019S (GS), are the most common cause of familial PD. LRRK2-PD has been associated with both αSyn and tau pathology; however the mechanistic links between LRRK2 dysfunction and protein aggregation remain incompletely defined. Here we opted to investigate whether LRRK2 contributes to αSyn and tau pathology through common molecular pathways or via distinct cellular mechanisms. Viral vector-mediated αSyn overexpression in GS LRRK2 knock-in mice led to enhanced dopaminergic neurodegeneration, increased phosphorylated αSyn levels, pronounced neuroinflammation, and accumulation of lysosomal proteins, suggesting impaired αSyn clearance and immune activation as key drivers. Human iPSC-derived dopaminergic neurons from GS LRRK2 PD patients mirrored these findings. In contrast viral vector-mediated overexpression of tau in GS LRRK2 knock-in mice promoted tau phosphorylation but did not significantly affect neuroinflammation, lysosomal markers, or neurodegeneration, indicating a primarily cell-autonomous mechanism. Our results reveal a mechanistic divergence in how GS LRRK2 impacts αSyn and tau pathologies, supporting the notion that LRRK2 kinase activity contributes to PD pathogenesis through different pathways, thereby highlighting its potential as a therapeutic target in both familial and sporadic PD.

Keywords Alpha-synuclein · LRRK2 · Parkinson's disease · Tau

George Tsafaras and Diego Cabezudo have equally contributed to this work

✉ Veerle Baekelandt
veerle.baekelandt@kuleuven.be

[1] Laboratory for Neurobiology and Gene Therapy, Department of Neurosciences, Leuven Brain Institute, KU Leuven, Herestraat 49 - 1023, 3000 Leuven, Belgium

[2] Oxford Parkinson's Disease Centre and Department of Physiology, Anatomy and Genetics, University of Oxford, Oxford OX1 3QU, UK

[3] VIB-KU Leuven Center for Brain and Disease Research, Leuven, Belgium

[4] Kavli Institute for Nanoscience Discovery, University of Oxford, Oxford OX1 3QU, UK

[5] Leuven Viral Vector Core, KU Leuven, Herestraat 49 - 1023, 3000 Leuven, Belgium

Abbreviations

PD	Parkinson's disease
LB	Lewy bodies
LN	Lewy neurites
αSyn	Alpha-Synuclein
LRRK2	Leucine-rich repeat kinase 2
GS	G2019S
CSF	Central nervous system
SN	Substantia nigra
AD	Alzheimer's disease
PFF	Pre-formed fibril
rAAV	Recombinant adeno-associated viral
WT	Wild-type
KI	Knock-in
fLuc	Firefly Luciferase vector
PFA	Paraformaldehyde
PBS	Phosphate buffered saline
RT	Room temperature
PBS-T	PBS with 0.1% Tergitol

Published online: 11 November 2025

DAB	3' Diaminobenzidine tetrahydrochloride
TH	Tyrosine hydroxylase
TBS	Tris buffered saline
TBS-T	TBS with 0.1% Tween-20
pS129	Phosphorylated S129
HBSS	Hank's Balanced Salt Solution
DMEM	Dulbecco's Modified Eagle Medium
FBS	Foetal bovine serum
MHCII	Major histocompatibility complex II
iPSC	Induced pluripotent stem cell
DIV	Day in vitro
LV	Lentiviral vector
SD	Standard deviation
dSTR	Dorsal striatum
NK	Natural killer
IL	Interleukin
IFN	Interferon
TNF-α	Tumour Necrosis Factor-α
TFEB	Transcription factor EB
GSK3b	Glycogen synthase kinase-3 beta
Cdk5	Cyclin-dependent kinase 5
MFI	Mean fluorescence intensity

Introduction

Parkinson's disease (PD) is the second most common neurodegenerative disorder, affecting 6–10 million people worldwide. The disease is characterised by a progressive loss of dopaminergic neurons in the substantia nigra pars compacta (SN), resulting in motor symptoms, including rigidity, postural instability, tremor and bradykinesia [10]. The main histopathological feature of the disease is the presence of intraneuronal protein aggregates termed Lewy bodies (LB) and Lewy neurites (LN) [28, 83]. LBs have been described as a crowded environment of membranes, including vesicular structures, dysmorphic organelles and proteins [78].

Mutations in genes encoding proteins such as alpha-synuclein (αSyn) and leucine-rich repeat kinase 2 (LRRK2) have been linked with familial and sporadic PD cases. LRRK2 is a complex multi-domain protein with kinase and GTPase enzymatic activity. Familial PD cases are most commonly caused by mutations in the LRRK2 gene, and further variants at the LRRK2 locus have been associated with an enhanced risk of developing sporadic PD [60]. All LRRK2 pathogenic mutations identified have been shown to increase the kinase activity of the protein. Although the prevalence differs considerably across ethnicities and geographical populations, the G2019S (GS) mutation remains the most common LRRK2 variant in familial and sporadic PD worldwide [33]. While αSyn is the major component of LBs and LNs, tau is mostly associated with tauopathies such as Alzheimer's disease (AD) and frontotemporal dementia, where it is hyperphosphorylated and accumulates in neurofibrillary tangles. However, tau has also been detected in the brains of PD [78, 89].

Emerging evidence suggests that LRRK2 has a central role in the pathogenesis of PD. LRRK2-PD has been associated with both αSyn pathology and tau [89]. Several lines of research have investigated the role of each pathology, but the results have been contradictory. Examining the interaction between LRRK2 and αSyn, it has been reported that around 50% of LRRK2 PD patients lack the typical LBs [44] and are less likely to be positive in a cerebrospinal fluid (CSF) αSyn seed amplification assay [80]. On the other hand, LRRK2 levels in PD brain samples were positively associated with increased αSyn phosphorylation and aggregation in affected brain regions [34]. The manifestation of LRRK2-related pathology appears to be mutation dependent, with some variants like G2019S displaying both αSyn and tau co-pathology, while others, such as I2020T, are predominantly linked to tau pathology [55, 71, 97]. Interestingly, significantly higher levels of αSyn oligomers have been found in the CSF of symptomatic LRRK2 mutation carriers compared to healthy controls [1, 53]. Two recent studies using proximity ligation assay have reported that in all LRRK2 PD cases tested, αSyn oligomers were present regardless of LB pathology [43, 77]. Moreover, animal studies have shown ameliorated αSyn neuropathology and neurodegeneration after LRRK2 inhibition or deficiency [18, 20, 50, 88], while others failed to report neuroprotection [3, 19, 39, 67, 96]. With regard to tau, post-mortem studies of LRRK2 PD patients have reported that the majority consistently exhibit tau pathology [11, 40, 51, 69]. Interestingly, overexpression of different LRRK2 mutations both in the dopaminergic neurons of the SN of rats and primary cortical neurons induced phosphorylated tau positive inclusions, leading to increased cellular death [52]. In GS LRRK2 transgenic mice tau overexpression in the hippocampal CA1 region led to enhanced neuron-to-neuron transmission but did not affect tau phosphorylation [62]. Similarly, after injection with tau aggregates from AD patients an elevated retrograde transmission of tau pathology was demonstrated in the presence of GS LRRK2 [16]. Nevertheless, another study did not detect differences in tau pathology between primary neurons expressing GS LRRK2 and WT LRRK2 after exposure to tau pre-formed fibrils (PFFs) [37].

LRRK2 has been described to play a role in several cellular processes including mitochondrial homeostasis, lysosomal acidification, autophagy/mitophagy and neurite outgrowth [54, 66, 72, 81, 90] Particularly, lysosomal distress has been widely described in PD and has been associated with enhanced LRRK2 kinase activity. Several LRRK2-interacting proteins including auxilin, ATP13A2, LAMP2a, and ArfGAP1 are linked with lysosomal dysregulation [41, 56, 63, 65, 84]. In addition, the D290N VSP35 mutation and

GBA1 mutations, such as N370S and E326K, both associated with endolysosomal dysfunction, have been shown to enhance LRRK2 kinase activity [58, 93]. LRRK2 regulates cytoskeletal dynamics and, under pathological conditions, can disrupt vesicular trafficking by blocking motor proteins that depend on microtubules for transport [4].

While early research was predominantly neuron-centric, LRRK2 is now recognised to play important roles beyond the central nervous system. Over the past decade, an extensive body of work has demonstrated the involvement of LRRK2 in immune cell biology. LRRK2 is highly expressed in myeloid cells and to a lesser extent in B and T cells, suggesting that it may play a critical role in regulating inflammation [15, 31, 36, 86]. Given that the central nervous system is less immune-privileged than previously believed, inflammatory pathways may serve as a mechanistic link between LRRK2 and PD pathology. LRRK2 mutations, including the GS, have been linked with stronger pro-inflammatory responses both in patients and in vivo models for PD [25, 75]. Moreover, under inflammatory conditions immune cells seem to demonstrate increased expression and activity of LRRK2 [74].

Here, we aimed to further clarify the link between GS LRRK2 and αSyn or tau-mediated neurodegeneration in vivo by utilising our in-house recombinant adeno-associated viral (rAAV) vector PD models. In our previous studies, we have shown that αSyn overexpression using rAAV models can lead to progressive neurodegeneration, neuropathology, and neuroinflammatory alterations in the SN of rodents, changes that are observed in a time- and dose-dependent manner [64, 67, 68]. Here, we induced overexpression of wild-type (WT) human αSyn or human full-length tau in the SN of GS LRRK2 knock-in (KI) and WT mice and studied the impact of the mutation on disease pathophysiology. The 2N4R tau isoform is the major form expressed in the adult brain. Although mixed 3R/4R tau species are observed in PD, the relative abundance of 4R tau tends to increase, similar to the 4R:3R imbalance reported in AD. We opted to use this isoform to model tau pathology in this study, also based on its robust aggregation and neurotoxicity in vivo [13, 95]. We found that the gain-of-function GS mutation exacerbates both αSyn and tau neuropathology in our models. We report that αSyn pathology is accompanied by a pro-inflammatory environment in the brain of the GS mice, with enhanced recruitment of peripheral immune cells as well as high levels of cytokines. We also associated the aggravated αSyn pathology in the GS LRRK2 mice with disturbances in lysosomal proteins. Interestingly, after 2N4R tau overexpression we detected higher levels of hyperphosphorylated tau in GS mice, which can infer the aggravated neuropathology, but in the absence of significant neuroinflammation. Finally, we further confirmed that the presence of GS LRRK2 induces more αSyn pathology in PD patient induced pluripotent stem cell (iPSC)-derived dopaminergic neurons. Our results provide more insight into the pathological function of GS LRRK2 and suggest the possible involvement in different mechanistic pathways regulating αSyn and tau neuropathology.

Materials and methods

Animals and ethical approval

The animal experiments conducted in this study were in compliance with the European Communities Council Directive of November 24, 1986 (86/609/EEC) and were authorised by the Bioethical Committee of the KU Leuven (Belgium) under ECD project 051/2020. Male C57BL/6 J (NTG, JAX 000664, RRID: IMSR_JAX:000664) and B6.Cg-Lrrk2tm1.1Hlme/J (GS LRRK2, JAX:030961, RRID:IMSR_JAX:030961) aged between 8 and 10 weeks were utilised for this study. All wild-type controls in this study were littermates derived from the LRRK2 KI breeding colonies, thus ensuring a matched genetic background. These animals were housed in individually ventilated cages and provided free access to food and water, with a controlled light–dark cycle (12 h light–12 h dark) and temperature (21 ± 1 °C).

Stereotactic injections

The surgical procedures performed in this study adhered to aseptic techniques, and the animals received anaesthesia with ketamine (60 mg/kg, i.p., Ketalar, Pfizer, Puurs) and medetomidine (0.4 mg/kg, Dormitor, Pfizer). Once the anaesthesia took effect, the mice were placed in a stereotactic head frame (Stoelting, Wood Dale, IL), and injections were performed using a 30-gauge needle and a 10-µl Hamilton syringe (Hamilton, Bonaduz, GR, Switzerland). GS LRRK2 or WT mice were injected with 2 µl saline or rAAV2/7 αSyn vector (CMVenh-Synapsin-intron-Hs αSyn WT) at a dose of 3 E + 9 genome copies or rAAV2/7 Tau vector (CMVenh-Synapsin-intron-Hs tau 2N4R) at a dose of 0.55 E + 8 genome copies per animal. As control a rAAV2/7 firefly Luciferase vector (fLuc) (CMVenh-Synapsin-intron-luciferase) was used at a dose of 3 E + 9 genome copies. The right SN was targeted using the following stereotactic coordinates: anteroposterior −3.1 mm, mediolateral −1.2 mm, and dorsoventral 4.3 mm using bregma as a reference. The injection was delivered at a rate of 0.25 µl/min, with a 5-min interval following initial needle placement. The needle remained in place for an additional 5 min after the injection before being slowly retracted.

Behavioural analysis

Behavioural tests were used to evaluate motor asymmetry and motor function at 2, 4, 8, and 14 weeks post-injection. For each test, mice were acclimatised to the testing room at least 1 h prior to assessment. Automated systems were used for the rotarod and open-field tests. Quantification of the videos for the other tests was done by a blinded researcher. Motor coordination and balance were evaluated using an accelerated rotarod system (IITC Life Science Rotarod Model I-755, Campden Instruments). Mice were placed on rotating rods and were allowed to walk face forward under steady rotation speed (4 rpm) for at least one min. During this initial training time, mice were placed back on the rod after falling. Following training time, the speed of the rotation was progressively increased from 0 to 40 rpm over 120 s, while latency to fall or passive rotation was recorded. Three 5-min trials were conducted with 1 h resting intervals in between. The average latency for all trials was used for statistical analyses. Spontaneous locomotor activity was assessed with the open field test. The set-up consisted of a square box (50 × 50 cm) surrounded by opaque walls that prevent observation of visual cues outside the arena. Mice were placed separately in the centre of an arena and spontaneous locomotor activity was recorded using an overhead camera for 30 min. Total distance travelled, velocity, % immobility, and ipsi-/contralateral 180° turning time were obtained using AnimalTracker [35]. The cylinder test was employed to quantify asymmetry in forelimb use. Contacts made by each forepaw with the wall of a 20-cm-wide clear glass cylinder were scored from the videotapes by an observer. A minimum of 20 contacts was recorded and quantified for each animal.

Immunostaining and fluorescence-based analyses

Mice were sacrificed with an overdose of sodium pentobarbital (200 mg/kg, i.p., Dolethal, Vetoquinol) followed by intracardial perfusion with saline and 4% paraformaldehyde (PFA) in phosphate buffered saline (PBS). Isolated brains were post-fixed overnight in 4% PFA, and 25 µm-thick coronal brain sections were made with a vibrating microtome (HM 650 V, Microm). Immunohistochemistry was performed on free-floating sections using antibodies against the target proteins. Sections, after washed with PBS, were incubated in an antigen retrieval solution (0.1 M citrate buffer pH 6.0) for 30 min at 80°. After 20 min on ice, the sections were washed in PBS, and were treated with 3% hydrogen peroxide and 10% methanol in PBS for 10 min at room temperature (RT). For the proteinase K treatment, a 1 min incubation with the protease solution (20 mg/mL) was added, followed by 3 × 5 min washes in PBS, according to the manufacturer's instructions (Proteinase K, Thermo Fisher Scientific, EO0491). Then sections were washed 3 × 5 min in PBS with 0.1% Tergitol (PBS-T) and incubated overnight at RT with primary antibody in 10% goat or donkey serum (DakoCytomation).

For immunohistochemistry, the next day, after 3 × 5 min washes in PBS-T, the sections were incubated with biotinylated secondary antibody (biotinylated goat anti-rabbit IgG secondary antibody, DakoCytomation, ab6720) for 2 h at RT followed by incubation with streptavidin–horseradish peroxidase complex (P039701-2, Agilent) for 2 h at RT. Tyrosine hydroxylase (TH) immunoreactivity was visualised using Vector SG (SK-4700, Vector Laboratories) and IBA1 using 3,3' diaminobenzidine tetrahydrochloride (DAB; Merck Life Science BV, D5905).

For fluorescent staining, the second day the sections after washed 3 × 5 min in PBS-T were incubated in the dark for 2 h in fluorochrome-conjugated secondary antibodies. Then sections were rinsed in PBS mounted, and allowed to dry until coverslipped with Mowiol (47,904, Millipore).

For immunocytochemistry of the iPSCs, cells were fixed in 4% PFA at RT for 20 min and then stored at 4 °C in PBS, protected from light. Cells were permeabilised using 0.05% saponin in Tris buffered saline with 0.1% Tween-20 (TBS-T) for 30 min. Cells were then blocked with 10% normal donkey serum in TBS-T for 40 min, and incubated in primary antibodies in 1% serum in TBS-T overnight at 4 °C. Cells were then washed 3 times in TBS, incubated in secondary antibodies for 1 h, and then washed once in TBS before a 15-min incubation with 1 µg/mL DAPI. Cells were then washed 2 additional times before storage at 4 °C, protected from light.

For immunohistochemistry TH (rabbit, Millipore, AB152, 1:10.000) or Iba1 (rabbit, Abcam, ab178846, 1:5.000) primary antibodies were used. For immunofluorescent staining the following primary antibodies were used: GFAP (chicken, Abcam, ab4674, 1:1000); CD68 (rabbit, Invitrogen, PA5-83,940, 1:500); Iba1 (goat, Abcam, Ab5076, 1:500); TH (chicken, Aves Labs, TYH, 1:1000); TH (sheep, Millipore, ab1542, 1:1000); Neun (chicken, Millipore, ABN91, 1:1000); phosphorylated αSyn S129 (rabbit, Abcam, Ab51253, 1:1000); tau AT8 (mouse, Invitrogen, MN1020, 1:500); PHF1 (mouse, provided by Peter Davis, 1:500); total tau (rabbit, Dako, A0024, 1:1000).

The secondary antibodies used were Donkey anti-chicken Alexa 488 (Invitrogen, A78948, 1:500); Donkey anti-mouse Alexa 488 (Invitrogen, A21202, 1:500); Donkey anti-chicken Alexa 555 (Invitrogen, A21437, 1:500); Donkey anti-rabbit Alexa 555 (Invitrogen, A31572, 1:500); Donkey anti-rat Alexa 555 (Abcam, Ab150154, 1:500); Donkey anti-sheep Alexa 555 (Invitrogen, A21436, 1:500); Donkey anti-goat Alexa 647 (Invitrogen, A21447, 1:500); Donkey anti-rabbit Alexa 647 (Invitrogen, A32795; A21245, 1:500); Donkey anti-mouse Alexa 647 (Invitrogen, A31571, 1:500).

Stereological quantification of dopaminergic neurons

To evaluate the SN integrity, the number of TH + cells was counted using stereological measurements with the optical fractionator method on a computerised system, as previously described [8] using Stereo Investigator by MicroBrightField, Delft, The Netherlands. A total of five sections from each animal were analysed for TH immunoreactivity, selecting every 8th section throughout the entire SN, along the rostrocaudal axis. The coefficients of error were calculated using the Schmitz and Hof procedure to estimate precision, ranging from 0.05 to 0.10. The loss of dopaminergic neurons as a percentage injected compared to the non-injected, contralateral side was reported. All analyses were conducted by a blinded investigator for the different groups.

Flow cytometry

The animals were euthanised with an overdose of sodium pentobarbital (Dolethal, 200 mg/kg, i.p.) and subjected to intracardial perfusion with ice-cold saline. The SN was isolated and enzymatically digested with Collagenase D (Merck Life Science BV) and DNAse I (Roche) at 37 °C, and then passed through a 70 µm cell strainer. The cells were washed with Hank's Balanced Salt Solution (HBSS) and centrifuged at 1000 g for 10 min. The pellet was suspended in 38% Percoll (GE Healthcare Bio-Sciences) and centrifuged for 25 min at 800 g with slow acceleration and no brake. The cell pellet was collected and washed once with Dulbecco's Modified Eagle Medium (DMEM) containing 10% foetal bovine serum (FBS) and once in FBS stain buffer (BD Biosciences). Mouse anti-rat FcγII receptor (CD32) (D34-485, BD Biosciences) was used to block the cells in FBS stain buffer, and the following surface markers were stained: CD45 30-F11, PE-Cy7 (Biolegend); CD11b M1/70, PerCPCy5.5- (Biolegend); Ly-6G 1A8, PE (BioLegend); CD4 GK1.5, AlexaFluor 488 (BioLegend); CD8a 53–6.7, Pacific Blue (BioLegend); CD25 PC61, PE-Cy5 (BioLegend); major histocompatibility complex (MHC) II M5/114.15.2, APC (BioLegend); Ly-6C HK1.4, Brilliant Violet 605 (BioLegend); CD19 6D5, Brilliant Violet 570 (BioLegend); CD11c, eFluor 506 (ThermoFisher eBioscience); CD161 PK136, Brilliant Violet 650 (BioLegend); CD68 FA-11, Brilliant Violet 711 (BioLegend); CD3 17A2, Brilliant Violet 750 (BioLegend). In each condition it was included a fixable viability dye eFluor 780 (eBioscience). The cells were fixed in 10% formalin and analysed the next day. Flow cytometry/FACS was performed at the VIB-KU Leuven FACS Core Facility using a BD FACSymphony A5 cytometer with the FACSDiva software. Gating strategy is shown in Fig. Sup. 3. FlowJo v10.0.7 software was used for data analysis. From each sample 100,000 events were recorded.

Protein extraction

For protein analysis, mice were sacrificed and transcardially perfused only with saline. SN tissue was freshly isolated, weighted and snap-frozen at -80 °C. Samples were homogenised utilising a tissue homogeniser (TH, Omni Tissue Homogenizer) in 10 volumes of RIPA buffer (50 mM Tris–HCl, 150 mM NaCl, 0.1% (w/v) SDS, 1% (v/v) Triton-X100, 0.5% (w/v) sodium deoxycholate, 1.0 mM EDTA pH 7.4) containing protease inhibitor cocktail (Roche cOmplete) and phospho-STOP EASYPACK (Roche). The samples were then incubated for 20 min at 4 °C and centrifuged at 3000 g for 10 min at 4 °C. The resulting supernatant was further centrifuged at 20,000 g for 30 min at 4 °C, and the supernatants were used as the protein fraction. Left-over pellets were further processed for sarkosyl-insoluble faction extraction as previously described [32]. Pellets were pooled and homogenised using a FastPrep (Fisher Scientific, Merelbeke, Belgium) in cold buffer (10 mM Tris–HCl pH 7.4, 0.8 M NaCl, 1 mM EGTA and 10% sucrose), treated with Universal Nuclease (Pierce, ThermoFisher Scientific, MA, USA) and incubated for 30 min incubation at RT. Samples were then brought to 1% Sarkosyl (Sigma-Aldrich, Missouri, USA), incubated for 1 h with shaking, and centrifuged at 350,000 g for 1 h at 4 °C. The pellet was washed, recentrifuged, and resuspended in 50 mM Tris–HCl pH 7.4 (175 mg tissue/100 µL). The concentration of protein in the samples was determined using a BCA protein assay (Thermo Scientific) according to the manufacturer's instructions.

Western blot

Thirty µg of protein was loaded onto 4–15% Criterion TGX Precast Midi Protein Gel (Bio-Rad, 5,671,084) or 15% Criterion Tris–HCl Protein Gel (Bio-Rad, 3,450,020) to separate the proteins. Proteins were subsequently transferred onto polyvinylidene fluoride (PVDF) membrane (Bio-Rad, 1,620,174) and analysed by immunoblotting. Nonspecific binding sites were blocked for 1 h at RT in 5% non-fat milk in PBS-T for 1 h at RT and probed overnight at 4 °C with the following primary antibodies: total αSyn C20 (rabbit, sc-7011-R, Santa Cruz, 1:1000); anti-pS129 αSyn (rabbit, Abcam, ab51253, 1:1000); LAMP2A (rabbit, Abcam, ab18528, 1:500); LAMP1 (rabbit, Abcam, ab24170, 1:1000); GBA (rabbit, Sigma-Aldrich, G4171, 1:1000); Cathepsin D (rabbit, Cell Signalling, 2284, 1:1000); Cathepsin B (mouse, Abcam, ab58802, 1:500); Cathepsin H (goat, R&D systems, AF1013, 1:2000); Cathepsin L (rat, R&D systems, MAB9521, 1:500); TFEB (rabbit, Thermo Fisher Scientific, A303-673A, 1:100); P62 (rabbit, Proteintech, 55,274–1-AP

62, 1:1000); tau AT8 (mouse, Invitrogen, MN1020, 1:1000); tau S396 (rabbit, Abcam, Ab109390,, 1:5000); tau HT7 (mouse, Thermo Fisher Scientific, MN1000, 1:1000); GSK3β (1F7) (mouse, Santa Cruz Biotechnology, sc53931, 1:1000); phospho-GSK3β (Ser9) (rabbit, Cell Signalling, 9331S, 1:1000); Cdk5 (mouse, Santa Cruz Biotechnology, sc6247, 1:1000); PHF1 (mouse, provided by Peter Davis, 1:500); mc1 (mouse, provided by Peter Davis, 1:100); anti-vinculin (mouse, Sigma, V9131, 1:10,000); GAPDH (rabbit, Abcam, ab9485, 1:1000). Membranes were washed and incubated with horseradish peroxidase–conjugated secondary antibody (Agilent, AB_2617138, AB_2617137, 1:10.000) for 1 h, at RT. Bands were visualised using Clarity Western ECL (Bio-Rad, 1,705,061) or ECL Select Western Blotting Detection Reagent (Cytiva, GERPN2235) and developed with a GE ImageQuant 800 (GE Healthcare). Finally, densitometric analysis was conducted using ImageQuant software (GE Healthcare).

Meso scale V-plex assay

Pro- and anti-inflammatory proteins were analysed in the protein fraction of the midbrain homogenates using a 96-well V-PLEX Mouse cytokine 19-plex (Proinflammatory Panel 1 and Cytokine Panel-1) (#K15255D; Meso Scale). Each mouse SN extract (homogenised in RIPA buffer) was diluted ten-fold with diluents and incubated for 2 h at RT. After washing with 0.05% Tween-20 in 0.01 M PBS, the plates were incubated with detection antibodies for 2 h at RT. Data were generated from the V-PLEX Mouse cytokine 19-plex kits by washing away detection antibody solution and adding reading buffer to generate an electrochemiluminescence signal measured in a Meso Quickplex SQ120 (Meso Scale) and quantified with the Discovery Workbench 4.0 software.

Human iPSC-derived dopamine neuron production

Human induced pluripotent stem cells (iPSCs) used in this study (Table 1) were obtained from Oxford STEMBancc; the generation and characterisation of the iPSC lines from both healthy individuals and from PD patients carrying the GS LRRK2 mutation has been previously reported [14, 48]. iPSCs were cultured under feeder-free conditions on Matrigel (BD Biosciences) using mTeSR1 medium (StemCell Technologies). Differentiation into dopaminergic neurons was based on previously published protocols [94] incorporating modifications described in [91].

Two days prior to neuronal induction, iPSCs were dissociated to single cells and seeded onto Geltrex-coated (Life Technologies) plates at a density of 1.5×10^5 cells/cm^2. For the first 10 days, the cells were patterned toward a ventral midbrain precursor identity [94]. Following expansion until day in vitro (DIV) 11, the medium was replaced with Neurobasal medium containing, B27 supplement, and 2 mM L-glutamine (Life Technologies) to promote dopaminergic differentiation [94]. At DIV 20, cells were lifted with StemPro Accutase (Life Technologies) and replated on plates coated sequentially with Poly-L-Ornithine (Sigma) and Geltrex with 10 µM ROCK inhibitor (Y-27632, STEMCELL technologies) at a density of 2.5×10^5 cells/cm^2 and allowed to mature for an additional 20 days.

On DIV 20, cells were transduced with lentiviral vectors (LV) carrying αSyn-YFP (CMVenhSyn-αSyn-linker-eYFP-IRES-Puro); 2N4R tau-YFP (CMVenhSyn-HsTAU-linker-eYFP-IRES-Puro); YFP (CMVenhSyn-linker-eYFP-IRES-Puro), and at DIV 30, 5 µg/ml of αSyn or tau PFFs (StressMarq: SPR-322B, SPR-480E) were added to the cultures. All experiments were conducted until DIV 35 or DIV 40, while data were derived from three independent differentiations. The data from the corrected isogenic line (SFC832-03–06-C47) were analysed with the healthy control group.

Microscopy and image analysis

Immunohistochemical staining for TH and Iba1 were scanned using an Aperio ScanScope CS whole slide scanner at 20X magnification. Fluorescent staining images were acquired with Leica DM6 B upright microscope using Leica Application Suite 3.6 Download. For analysis of the SN, tiled images of 20–40 × magnification were obtained and analysed using QuPath 0.3.2. For images captured in

Table 1 Cell lines employed in this study

Disease	Sex	Age of Biopsy	Bio-bank	Line name	Reference
Healthy Control	M	72	StemBancc	SFC067-03–01	(Lang et al., 2019)
Healthy Control	M	75	StemBancc	SFC156-03–01	(Lang et al., 2019)
Healthy Control	F	78	StemBancc	SFC856-03–04	(Haenseler et al., 2017)
GS LRRK2 PD	M	49	StemBancc	JR036-1	(Connor-Robson et al., 2019)
GS LRRK2 PD	M	57	StemBancc	SFC855-03–06	(Connor-Robson et al., 2019)
GS LRRK2 PD	F	77	StemBancc	SFC832-03–06	(Connor-Robson et al., 2019)
GS LRRK2 PD-corrected	F	77	StemBancc	SFC832-03–06-C47	

Z-stacks 3D reconstruction was performed using Imaris version 10.0.1 (Oxford Instruments, Abingdon, United Kingdom), and the density of each marker was quantified as the number of voxels occupied by the respective channel normalised to the total number of voxels that corresponded to the delineated cell surfaces within the field of view.

The data from the iPSC-derived neurons were obtained via high-content confocal imaging on a Perkin Elmer Opera Phenix™, using a 40 × magnification water immersion objective. Typically, 20–30 images were acquired per well, and 3 wells were analysed per differentiation per cell line. The binning value used was 1–2 and 4–5 single focal plane were obtained. Images were analysed using Harmony analysis software (Version 5.2).

Statistical analysis

Graph creation and statistical analysis were performed using GraphPad Prism for Windows (GraphPad Software, Inc.), version 10.2.0. Results are presented as means ± standard deviation (SD) of the mean. Normality of data was tested using the Shapiro–Wilk test. Statistical significance was assessed using t-test or when multiple groups were analysed simultaneously, one-way ANOVA followed by Tukey's multiple comparison post hoc test or two-way ANOVA followed by Tukey's multiple comparison test. Significance was represented as follows: $*p<0.05$, $**p<0.01$, $***p<0.001$, and $****p<0.0001$. For the FACs and biochemical analysis the saline and fLuc-AAV were included as a minimal technical control ($n=2$ per genotype) to confirm the absence of unspecific AAV effects. Since they are not part of the main biological comparisons, they were not included in the statistical analysis.

Results

The G2019S LRRK2 mutation exacerbates αSyn-induced neurodegeneration and neuropathology in mice.

In this study, we first examined the effect of the GS LRRK2 mutation on αSyn neuropathology by comparing KI mice carrying the GS LRRK2 mutation and WT LRRK2 mice, obtained by the GS LRRK2 heterozygous breeding. To induce αSyn pathology we employed our in-house PD mouse model based on human αSyn overexpression in the SN using recombinant adeno-associated viral vectors (rAAV 2/7). This model induces progressive dopaminergic neurodegeneration, behavioural deficits and neuroinflammation [64]. Importantly these phenotypes are specific for αSyn, as none of them were detected in mice injected with a control vector encoding GFP [64]. In this study only male mice were used in order to reduce variability in time-sensitive analyses. We also previously found a reduced response to experimental colitis in female GS LRRK2 mice [12]. GS and WT LRRK2 mice were stereotactically injected with rAAV2/7 WT human αSyn vector (αSyn-rAAV) in the SN and sacrificed at two different time points, 4- and 14-weeks post-injection (Fig. 1a).

To evaluate the motor performance, we conducted behavioural tests including the cylinder and rotarod test at different times post injection. The cylinder test, used to measure the forelimb asymmetry, was applied longitudinally, every two weeks, for 14 weeks (Fig. 1b). We observed a progressive reduction in the use of the contralateral left paw which showed a non-significant trend of more impairment in the GS mice compared to controls. In the rotarod test, GS mice showed significantly compromised motor coordination and balance 4 weeks after αSyn-rAAV injection, as evidenced by the time spent on the rod compared to the WT mice (Fig. 1c).

Stereological counting of the TH + neurons in the SN corroborated the behavioural data, revealing a more significant loss in the number of TH + dopaminergic neurons in the ipsilateral compared to the contralateral SN in GS LRRK2 mice already 4 weeks post αSyn-rAAV injection. This difference remained significant at the 14 weeks timepoint (Fig. 1d–f). As the dopaminergic neurons extend axons to the dorsal striatum (dSTR) we performed quantification of TH optical density in the dSTR. Both at 4 and 14 weeks time point, we observed a stronger albeit non-significant increased loss of the dopaminergic terminals in the GS mice compared to the WT (Fig. 1g-i). Mice injected with a control firefly Luciferase vector (fLuc-rAAV) did not display loss of dopaminergic neurons or αSyn accumulation (Fig. Sup. 1a-d, h). Altogether, αSyn overexpression in the SN induces enhanced dopaminergic dysfunction in GS mice compared to WT mice.

Next, we characterised αSyn neuropathology using immunohistochemical approaches. The number and intensity of phosphorylated Serine 129 (pS129) αSyn positive cells were increased in the GS compared to WT mice in transduced nigral neurons in general and in TH + dopaminergic neurons specifically (Fig. 1j-n). In order to determine whether the pS129 αSyn corresponds to pathological aggregated or physiological phosphorylated αSyn species, we performed proteinase K pretreatment. This analysis revealed a similar increased trend in the number of positive cells and significantly higher pS129 αSyn-positive area in the GS mice (Fig. 1o-q). Further biochemical analysis from midbrain lysates confirmed the same pattern with significantly higher accumulation of total αSyn and a trend towards increased pS129 αSyn (Fig. Sup. 2). This suggests that GS LRRK2 regulates pathways involved in the accumulation or insufficient clearance of pathological αSyn species.

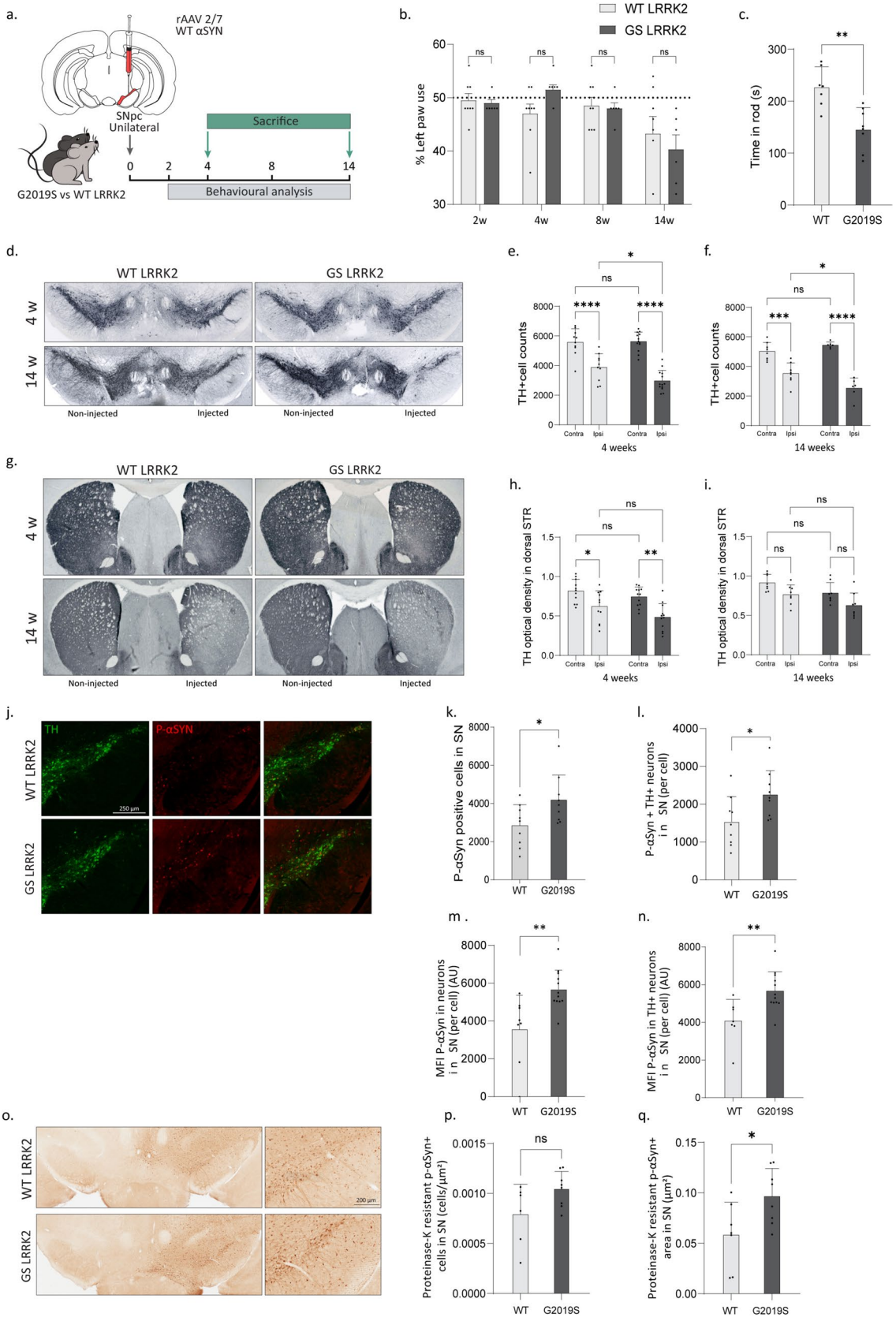
a.
rAAV 2/7
WT αSYN
SNpc
Unilateral
Sacrifice
0 2 4 8 14
Behavioural analysis
G2019S vs WT LRRK2
b.
WT LRRK2
GS LRRK2
% Left paw use
ns
2w 4w 8w 14w
c.
Time in rod (s)
WT G2019S
d.
WT LRRK2
GS LRRK2
4 w
14 w
Non-injected
Injected
e.
TH+cell counts
4 weeks
Contra Ipsi
f.
14 weeks
g.
h.
TH optical density in dorsal STR
i.
j.
TH
P-αSYN
250 µm
k.
P-αSyn positive cells in SN
l.
P-αSyn + TH+ neurons in SN (per cell)
m.
MFI P-αSyn in neurons in SN (per cell) (AU)
n.
MFI P-αSyn in TH+ neurons in SN (per cell) (AU)
o.
200 µm
p.
Proteinase-K resistant p-αSyn+ cells in SN (cells/µm²)
q.
Proteinase-K resistant p-αSyn+ area in SN (µm²)

◂**Fig. 1** The G2019S LRRK2 mutation exacerbates αSyn neuropathology and neurodegeneration upon αSyn overexpression in the SN. **a** Schematic representation of the experimental set up. WT and GS LRRK2 mice were unilaterally injected with αSyn rAAV 2/7 in the SN. WT control mice in this study were littermates derived from the LRRK2 KI breeding colonies, ensuring a matched genetic background. Mice were monitored behaviourally over time and sacrificed at 4 and 14 weeks post-injection. **b** Left forepaw use in the cylinder test for αSyn rAAV injected WT and GS LRRK2 mice. **c** Time to fall from the rotarod test 4 weeks post-injection. **d** Representative images of TH immunostaining in the SN 4 and 14 weeks post-injection of αSyn rAAV 2/7 injected WT and GS LRRK2 mice. **e**, **f** Stereological quantification of the DA neurons in the injected side and the non-injected side 4 and 14 weeks post-injection. **g** Representative images of TH immunostaining in the STR 4 and 14 weeks post-injection of αSyn rAAV 2/7 in WT and GS LRRK2 mice. **h**, **i** Quantification of the optical density of the TH + area in the dorsal striatum (STR) at 4 and 14 weeks post-injection in WT and GS LRRK2 mice. **j** Representative confocal images of TH + (green) and pS129 αSyn + (red) cells in the SN 4 weeks post-injection. Quantification of pS129 αSyn + **k** and pS129 αSyn + TH + **l** cells in the SN, as well as MFI of pS129 αSyn staining in neurons **m** and in TH + neurons **n** of the SN. Representative images of proteinase K resistant pS129 αSyn immunostaining in the SN 4 weeks post-injection **o**, and quantification of αSyn + cells **p** and αSyn + area **q** in the SN. N = 11–13 at the 4 weeks time point from two independent experiments, and N = 6–7 at the 14 weeks time point. Graphs represent mean ± SD. Statistical differences were assessed using unpaired Student's t-test or two-way ANOVA followed by Tukey's multiple comparison test. *$p < 0.05$, **$p < 0.01$, ***$p < 0.001$, ****$p < 0.0001$

The G2019S LRRK2 mice demonstrate increased inflammatory response upon αSyn overexpression

We have previously reported sustained neuroinflammation as one of the main phenotypes in our αSyn model [64, 67] (Fig. Sup. 2d, e). Importantly, LRRK2 is highly expressed in myeloid cells and to a lower extent in B and T cells and mutations such as the GS have been linked to enhanced pro-inflammatory responses both in patients and in vivo models for PD [24, 75]. Thus, we further investigated the impact of GS LRRK2 in regulating αSyn-induced immune response in our model.

To characterise the inflammatory status in the SN we first performed flow cytometry-based immunophenotyping (Fig. 2a). An overall increased inflammatory response was found in all mice injected with αSyn-rAAV compared to the fLuc-rAAV, confirming that αSyn acts as an inflammatory protein. Total numbers of myeloid cells (CD45hi, CD11b +) were significantly increased in the GS compared to WT animals. When looking at different subpopulations, we observed a significantly higher infiltration of neutrophils (Ly6G +) and a similar trend for classical (Ly6C +), non-classical (Ly6C–), and major histocompatibility complex II + (MHCII +) monocytes. No differences were detected for the lymphoid population (CD45hi, CD11b–), including B cells (CD19 +), CD4 + and CD8 + T cells. Interestingly, natural killer (NK) cells (CD3-CD161 +) were also significantly increased in the GS LRRK2 animals. To further refine alterations in the lymphoid population, we measured the CD25 surface marker in CD4 + T cells, which are typically considered as a subset of regulatory T cells [27]. The mean fluorescence intensity of CD25 in CD4 + T cells was remarkably reduced in GS LRRK2 mice injected with αSyn-rAAV compared to WT mice (Fig. 2b, c).

In addition, we measured cytokine levels in SN homogenates by multiplexed ELISA (MSD) (Fig. 2d, Fig. Sup. 4). An overall increase in cytokine levels was present in GS LRRK2 mice 1 month after injection of αSyn-rAAV. More specifically, significantly higher levels of interleukin-33 (IL-33), CCL2, CCL3, CXCL10, Interferon-γ (IFN-γ), IL-10, IL-1β, IL-2 and tumour necrosis factor-α (TNF-α) were detected compared to WT mice.

Finally, we characterised the astrocytes and microglia, the main resident immune regulators in the brain. One month post-injection, we performed immunohistochemistry for GFAP and IBA1, and quantified CD68 levels as a marker of microglial activation. Our data show that both WT and GS LRRK2 αSyn-rAAV-injected mice developed a strong inflammatory response in astrocytes and microglia in contrast to the fLuc-rAAV and the non-injected control group (Fig. 3a, Fig. Sup. 1e-g). Importantly, consistent with the pattern observed with the infiltrated peripheral immune cells, GS LRRK2 mice exhibited higher numbers of GFAP + astrocytes (Fig. 3a,b). The total number of IBA1 + cells was not different between WT and LRRK2 mice. However, quantification of the CD68 marker revealed a higher activation state of IBA1 + cells in the GS LRRK2 group (Fig. 3a, c, d). Overall, our data suggest a stronger immune response in the GS LRRK2 animals after αSyn overexpression in the SN.

LRRK2 G2019S mice demonstrate lysosomal protein accumulation after αSyn overexpression

LRRK2 has been repeatedly reported to play an important role in the endolysosomal pathway, including vesicle trafficking, autophagy, and lysosomal function [7, 85]. Disease-associated mutations in LRRK2, like the GS, have been implicated in disrupting lysosomal function, thereby contributing to the accumulation of misfolded proteins and inflammation [21, 73]. To address this, we quantified several lysosomal markers in the αSyn-rAAV injected mice. One month post-injection we detected a robust accumulation of lysosomal proteins in the SN of GS LRRK2 mice injected with αSyn-rAAV (Fig. 4). More specifically, we report a strong accumulation of cathepsins including cathepsin B, D, H, and L, as well as an accumulation of LAMP2a and LAMP1 (Fig. 4a-g). No differences were seen for other endolysosomal proteins such as p62, and Transcription factor EB (TFEB) (Fig. 4a, h, i). These findings reveal significant alterations in lysosomal function specifically upon αSyn

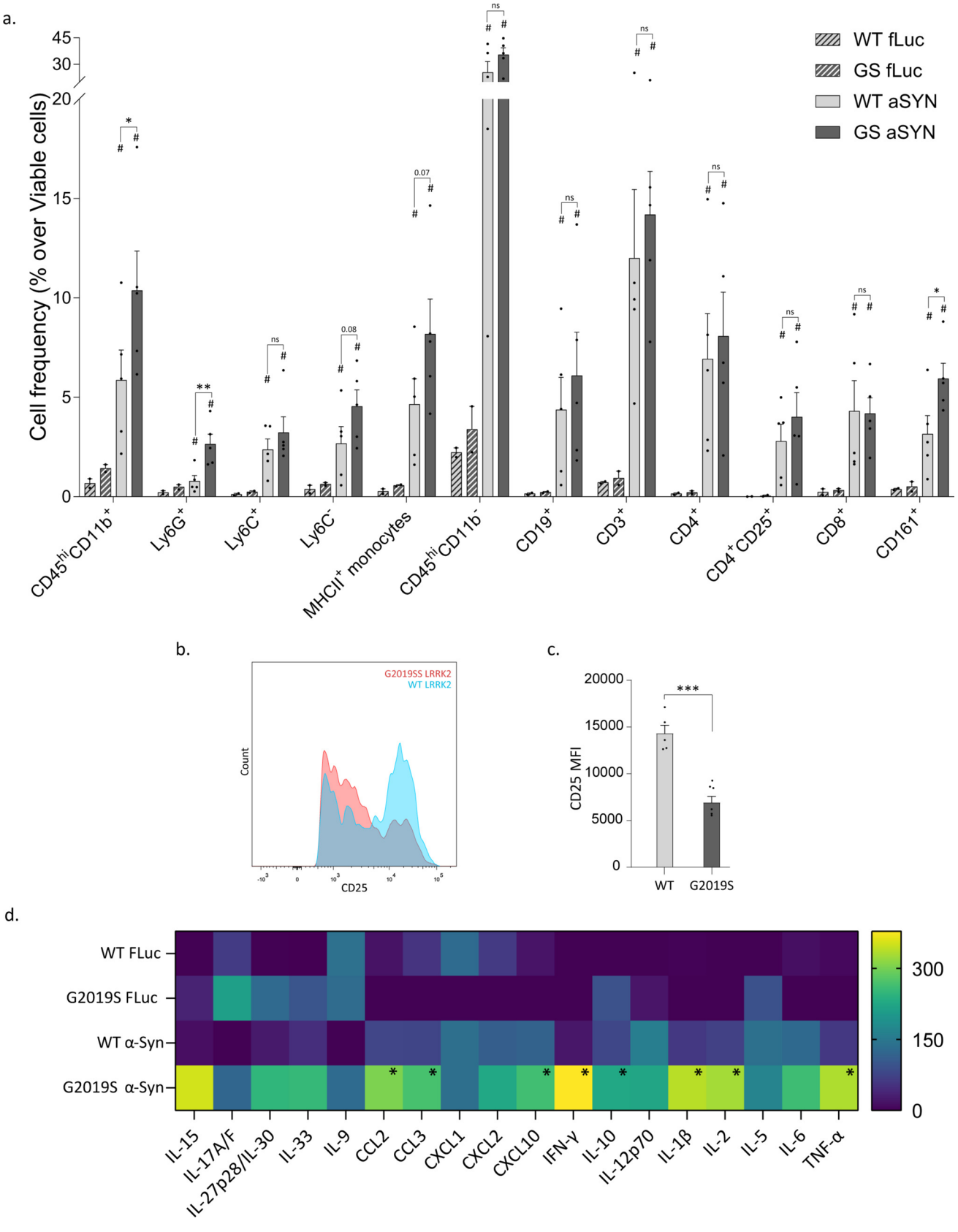
a.
Cell frequency (% over Viable cells)
WT fLuc
GS fLuc
WT aSYN
GS aSYN
CD45hiCD11b+
Ly6G+
Ly6C+
Ly6C-
MHCII+ monocytes
CD45hiCD11b-
CD19+
CD3+
CD4+
CD4+CD25+
CD8+
CD161+
b.
G2019SS LRRK2
WT LRRK2
Count
CD25
c.
CD25 MFI
WT
G2019S
d.
WT FLuc
G2019S FLuc
WT α-Syn
G2019S α-Syn
IL-15
IL-17A/F
IL-27p28/IL-30
IL-33
IL-9
CCL2
CCL3
CXCL1
CXCL2
CXCL10
IFN-γ
IL-10
IL-12p70
IL-1β
IL-2
IL-5
IL-6
TNF-α

◂**Fig. 2** Increased inflammatory response in the SN of G2019S mice after αSyn rAAV 2/7. **a** Immunophenotyping by flow cytometry of WT and GS LRRK2 mice 4 weeks post injection of αSyn/fLuc rAAV 2/7. Number of myeloid cells ($CD45^+$ $CD11b^+$), neutrophils ($Ly6G^+$), Ly6C + and Ly6C- monocytes, $MHCII^+$ monocytes, lymphocytes ($CD45^+$ CD11b), B cells ($CD19^+$), T cells (including $CD3^+$ mature T cells, $CD8^+$, $CD4^+$ and $CD4^+$ $CD25^+$), and natural killer cells ($CD161^+$). **b** Representative spectral emission profile of CD25 immunobinding and **c** quantification of CD25 immunoreactivity in $CD4^+$ $CD25^+$ cells in GS LRRK2 mice. **d** Quantification of pro-inflammatory cytokines in the injected SN 4 weeks post injection. Cytokines were measured in SN protein extracts from WT and GS LRRK2 mice after αSyn rAAV 2/7 injection and after control fLuc rAAV 2/7 injection. Increased levels of CCL2, CCL3, CXCL10, IFN-γ, IL-10, IL-1β, IL-2, and TNF-α were found in GS LRRK2 mice. N = 5 and graphs represent mean ± SD. Statistical differences were assessed using unpaired Student's t-test between WT and GS LRRK2 αSyn rAAV 2/7 injected groups. $*p < 0.05$, $**p < 0.01$

overexpression, suggesting a potential contributing mechanism through which GS LRRK2 exacerbates αSyn-induced pathology and neurodegeneration.

The G2019S LRRK2 mutation exacerbates tau pathology in mice

In order to get a better insight into the specificity of the GS LRRK2 effect towards αSyn, we decided to explore the effect of GS LRRK2 on tau neuropathology. Therefore, we induced tau overexpression in the SN of GS LRRK2 and WT mice using a similar viral vector approach (2N4R tau-rAAV). The mice were sacrificed at 4 and 8 weeks post-injection and characterised for dopaminergic neurodegeneration, behavioural deficits and neuroinflammation (Fig. 5a).

We investigated overall locomotor activity and exploration behaviour using the open field and evaluated different parameters including distance travelled and velocity (Fig. Sup. 5a, b). A progressive decline in both distance and speed was observed over time, but no significant differences were recorded between GS LRRK2 and WT mice. In the rotarod test, no significant differences in motor coordination and balance were observed between the groups at both time points (Fig. Sup. 5c). For forelimb asymmetry, we performed the cylinder test which only showed a mild impairment in the WT mice at 8 weeks (Fig. Sup. 4d).

We next quantified the TH + neurons in the SN of the tau-rAAV overexpression model and observed a progressive neuronal loss in the injected area. However, there was no difference in the loss of dopaminergic neurons between GS LRRK2 and WT mice at 4 or 8 weeks post-injection. (Fig. 5b-d). Quantification of the TH optical density in the dSTR, showed a progressive loss of the dopaminergic terminals between 4 and 8 weeks post-injection but no significant differences between GS and WT mice (Fig. 5c, d). Altogether, rAAV-mediated tau overexpression in the SN induces progressive loss of the dopaminergic neurons and terminals in the dSTR but this is not aggravated by the GS LRRK2 mutation. Mice injected with control fLuc-rAAV did not display loss of dopaminergic neurons or striatal terminals (Fig. Sup. 1a-d).

The G2019S LRRK2 mutation exacerbates tau phosphorylation upon tau overexpression

We then evaluated the effect of the GS LRRK2 mutation on tau neuropathology. We quantified the levels of different phosphorylated tau epitopes by immunohistochemical staining. With the AT8 tau antibody for p-tau S202 and Thr205, we observed a stronger signal in the nigral neurons of the GS LRRK2 mice compared to the WT (Fig. 6a, b). Also, higher levels of phosphorylated tau S396 and S404 as indicated by the PHF-1 antibody were detected in the GS LRRK2 mice (Fig. 6c-e). Western blot analysis from midbrain lysates confirmed similar effects on phosphorylated tau species. The bands for tau AT8 and for pTau S396 detected at different molecular weights depending on the conformation status and the isoform of the protein were significantly increased in the GS LRRK2 mice (Fig. 6f-l). Particularly, the 70 kDa band, where the 2N4R isoform is more enriched, showed consistently higher accumulation in GS LRRK2 mice. No significant increase in total tau species was detected (Fig. 6j). The ratio of p-tau S396 to total tau protein was still significantly higher (Fig. 6k). Further characterisation of the sarkosyl-insoluble fraction revealed no significant differences between WT and GS LRRK2 mice in any of the pathological tau forms tested, including p-tau species and conformation-specific epitopes (Fig. Sup. 5e-k).

To validate whether GS LRRK2 is involved in tau phosphorylation via regulation of tau kinases, we quantified the levels of two major tau kinases: glycogen synthase kinase-3 beta (GSK3b) and cyclin-dependent kinase 5 (Cdk5). There were no significant differences in total GSK3b and Cdk5 levels between GS LRRK2 and WT mice injected with tau-rAAV. Looking at phosphorylated GSK3b, which is the inactive form of the protein, we observed a non-significant decrease ($p = 0.06$) (Fig. 6f, m–o). This may suggest that increased LRRK2 kinase activity can regulate pathways associated with tau phosphorylation in neurons.

Tau overexpression does not induce neuroinflammation in mice

Since rAAV-mediated αSyn overexpression induces a strong neuroinflammatory response in GS LRRK2 mice (Figs. 2, 3), we wanted to characterise the effect of 2N4R tau-rAAV in the SN of these mice. We performed immunohistochemical staining in the SN at 1 month post-injection for GFAP, IBA1, and CD68 as a marker of microglial activation (Fig. 7). Remarkably, based on the quantification of these

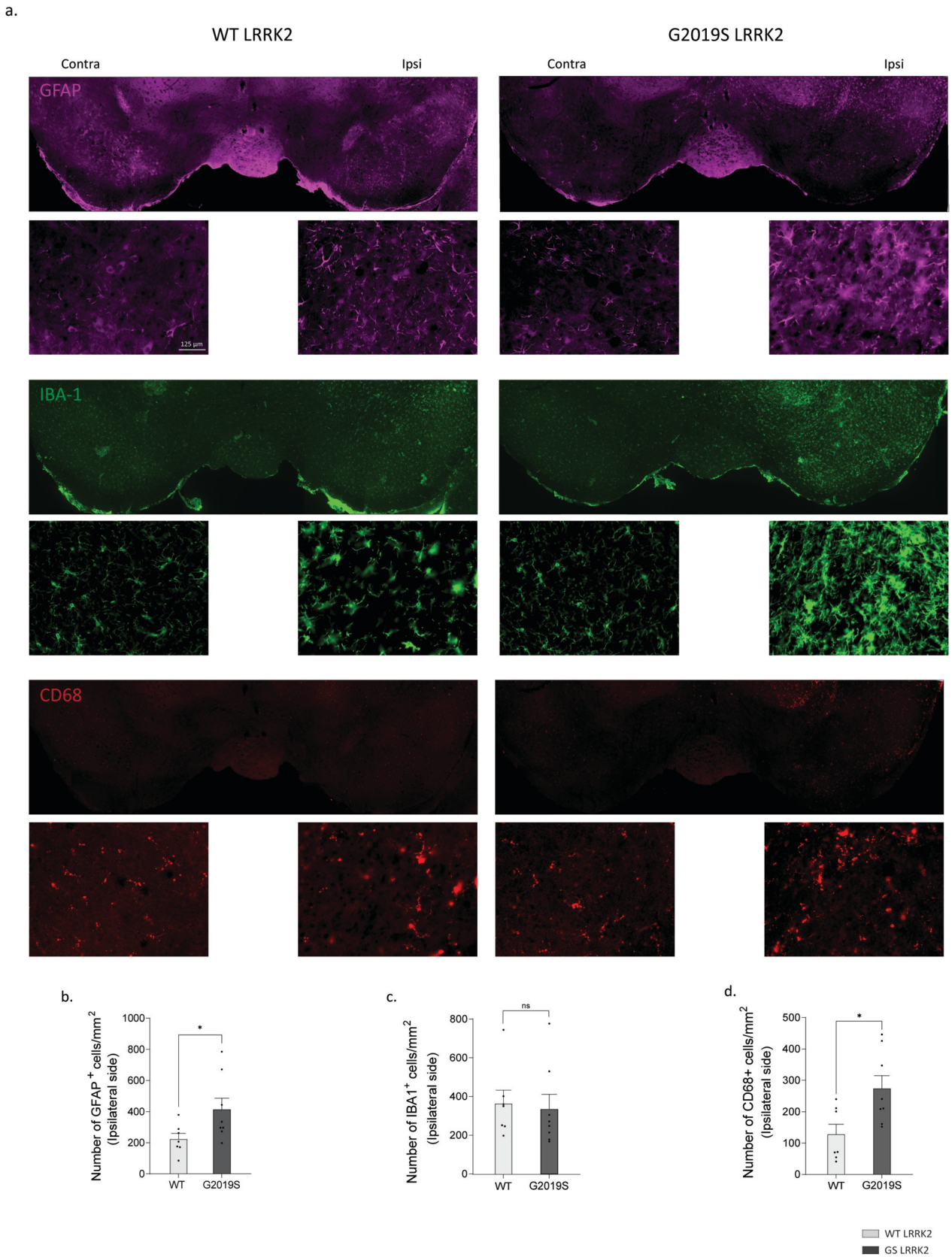
a.
WT LRRK2
G2019S LRRK2
Contra
Ipsi
Contra
Ipsi
GFAP
125 µm
IBA-1
CD68
b.
Number of GFAP+ cells/mm2 (Ipsilateral side)
1000
800
600
400
200
0
*
WT
G2019S
c.
Number of IBA1+ cells/mm2 (Ipsilateral side)
800
600
400
200
0
ns
WT
G2019S
d.
Number of CD68+ cells/mm2 (Ipsilateral side)
500
400
300
200
100
0
*
WT
G2019S
WT LRRK2
GS LRRK2

◂**Fig. 3** Immunohistochemical characterisation of the inflammatory response in the SN of G2019S mice after αSyn rAAV 2/7. Representative images **a** and quantification of astrocytes (GFAP) **b**, microglia (IBA1) **c**, and CD68 immunoreactivity **d** in the SN from WT and GS LRRK2 mice 4 weeks post injection. N = 7–8 and graphs represent mean ± SD. Statistical differences were assessed using an unpaired Student's t-test. *$p < 0.05$. Additional comparisons between animals of the same genotype injected with either αSyn rAAV2/7 or fLuc rAAV2/7 were performed using an unpaired Student's t-test. #$p < 0.05$ versus the respective fLuc group

3 markers, tau overexpression did not induce a significant neuroinflammatory response compared to the non-injected side similar to mice injected with the control fLuc-rAAV (Fig. 7, Fig. Sup. 5 l, m, Fig. Sup. 1e-g). Also, no differences were detected between GS LRRK2 and WT mice (Fig. 7a-d).

Characterisation of lysosomal markers in G2019S LRRK2 mice upon tau overexpression

Next, we investigated whether dysfunction in the endolysosomal pathway contributes to the regulation of tau proteinopathy in GS LRRK2 mice. We quantified several lysosomal markers similarly to those in the αSyn-rAAV injected mice. One month post tau-rAAV injection we did not detect aberrant accumulation of the lysosomal proteins Cathepsin H and L, Lamp1, Lamp2A, TFEB, or p62 in the SN of LRRK2 mice (Fig. 8a, c-j). Only cathepsin B levels appeared significantly upregulated in the SN of WT mice injected with tau-rAAV while significantly decreased in the GS LRRK2 mice (Fig. 8a, b).

LRRK2 G2019S promotes αSyn but not tau phosphorylation in dopaminergic neurons from human iPSC-derived midbrain culture

To explore the effect of the GS LRRK2 mutation on αSyn and tau pathology in a more translational model, PD patient-derived iPSC lines carrying the pathogenic GS LRRK2 mutation were used (Figs. 9, 10). Cells were differentiated into midbrain dopaminergic neurons and either αSyn or tau overexpression was induced via lentiviral vector (LV) transduction on day 20 of differentiation. Ten days later (DIV 30), cells were treated with recombinant αSyn or tau PFFs respectively to induce seeding of aggregation. We first examined whether the iPSC-derived dopaminergic neurons showed accumulation of pS129-αSyn or AT8-positive tau. We found an increased mean fluorescence intensity (MFI) of the pS129 αSyn spots in TH + neurons from GS LRRK2 PD patients compared to controls upon αSyn overexpression or the combination of αSyn overexpression with αSyn PFFs treatment (Fig. 9). In contrast, the same lines did not demonstrate different levels of tau AT8 MFI in TH + neurons after treatment with tau LV and tau PFFs (Fig. 10).

Discussion

Mutations in the LRRK2 gene are the most common cause of familial PD, and variants have also been identified in sporadic PD. Despite years of research, many questions remain unanswered regarding the pathogenic mechanism of these mutations. One key question is whether hyperactive LRRK2 interacts with αSyn or both proteins act in parallel to induce pathology. A direct interaction between these two proteins, such as αSyn being a substrate of LRRK2, has never been confirmed [23, 34, 50, 70]. Although some LRRK2 PD patients lack LB pathology and show reduced αSyn seeding in CSF [44, 80], αSyn oligomers are consistently elevated in mutation carriers [43, 77] suggesting that LRRK2 may modulate αSyn pathology even in the absence of classical LB inclusions. Considering that αSyn oligomers have been proposed as the most neurotoxic form of αSyn and control the nucleation process [5, 17, 87, 92], the question arises as to whether LRRK2 can regulate αSyn pathology at this oligomeric state.

A second crucial question revolves around tau pathology. Given that αSyn is not consistently observed as the primary neuropathological hallmark in LRRK2 patients, and considering the frequent detection of tau pathology, tau accumulation could contribute to the observed neurodegeneration. Our study demonstrates that the GS mutation in *LRRK2* exacerbates both αSyn and tau-mediated neuropathology in vivo, and enhances pathological aggregation of αSyn in human iPSC-derived dopaminergic neurons.

Research on αSyn-LRRK2 rodent models has shown variable and often contradictory outcomes [3, 18–20, 38, 50, 67, 88, 96]. A key limitation of some of these studies is their reliance on different αSyn models, particularly PFFs, which model aggregate propagation rather than early accumulation and aggregation mechanisms. To address these inconsistencies, we used our previously validated viral vector-mediated αSyn overexpression model that robustly induces progressive αSyn accumulation and aggregation, dopaminergic neurodegeneration, and neuroinflammation in the SN [64, 67]. This model allowed us to assess early and late disease stages in GS LRRK2 KI mice. In line with our hypothesis, αSyn overexpression in GS LRRK2 mice resulted in significantly greater dopaminergic neuron loss, earlier motor deficits, and higher levels of phosphorylated αSyn compared to WT controls. Importantly, similar findings were obtained in iPSC-derived dopaminergic neurons from GS LRRK2 PD patients, supporting the mutation's role in αSyn pathology.

The pS129 αSyn accumulation in the mice was accompanied by a robust pro-inflammatory response, including

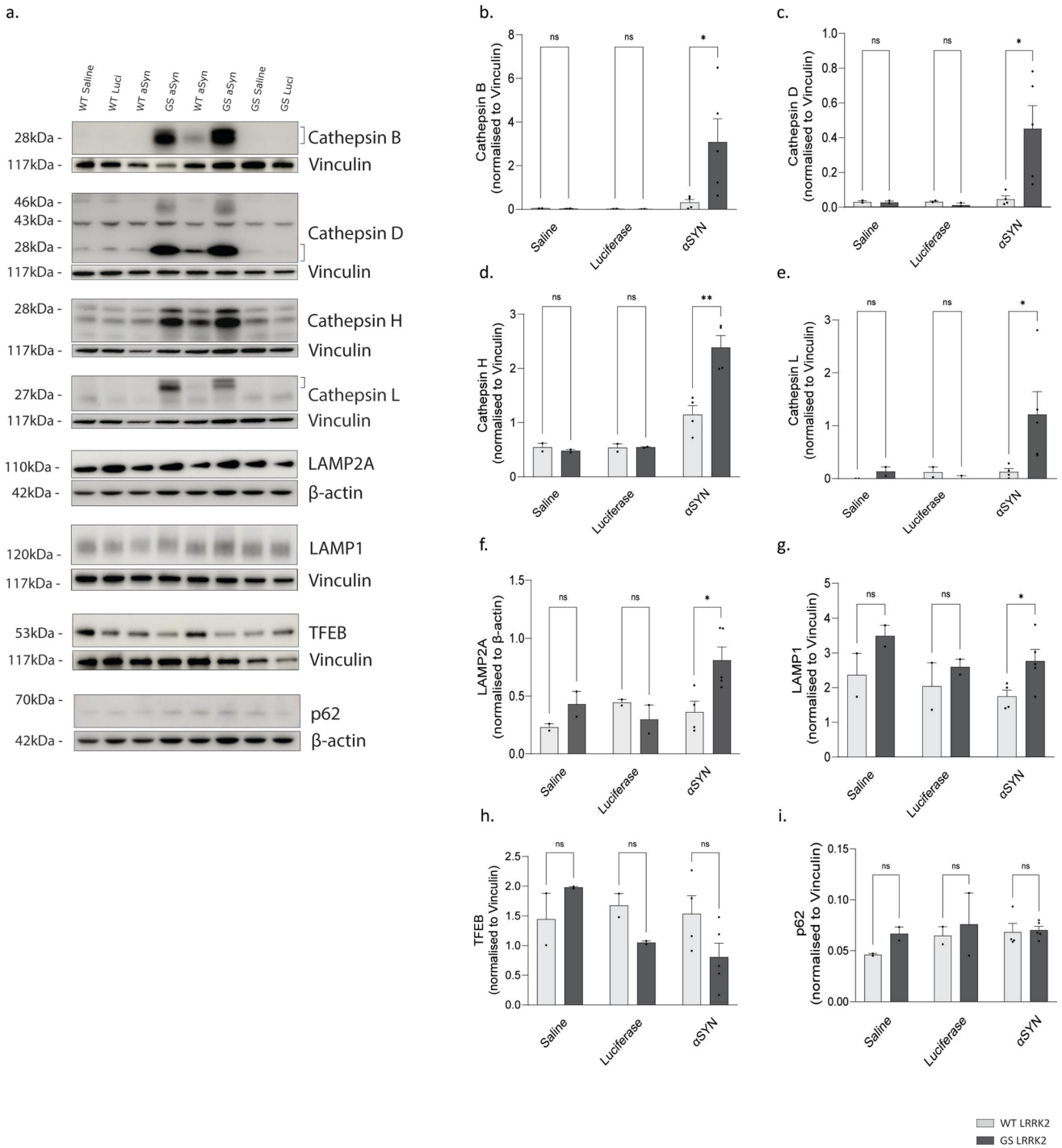

Fig. 4 LRRK2 G2019S mice demonstrate lysosomal protein accumulation upon αSyn overexpression in SN. **a** Representative western blot images from whole SN protein extracts from WT and GS LRRK2 mice 4 weeks post injection with αSyn rAAV 2/7 and control groups (fLuc rAAV 2/7 or saline injected mice). Immunoblots for Cathepsin B,D,H,L and, Lamp2a, Lamp1, TFEB, and p62 are shown. **b-i** Quantification of immunoblots. Values were normalised to the endogenous protein (vinculin or β-actin) levels. N = 4–5 for αSyn rAAV 2/7 groups and N = 2 for the control groups. Graphs represent mean ± SD. Statistical differences were assessed using unpaired Student's t-test. *$p < 0.05$, *** $p < 0.001$

increased infiltration of myeloid, neutrophils, and natural killer cells, elevated cytokine production, and reactive gliosis. Notably, we observed considerable dysregulation of lysosomal markers in GS LRRK2 mice, with upregulation of multiple cathepsins LAMP1, and LAMP2A, while TFEB and p62 remained unchanged. These results suggest

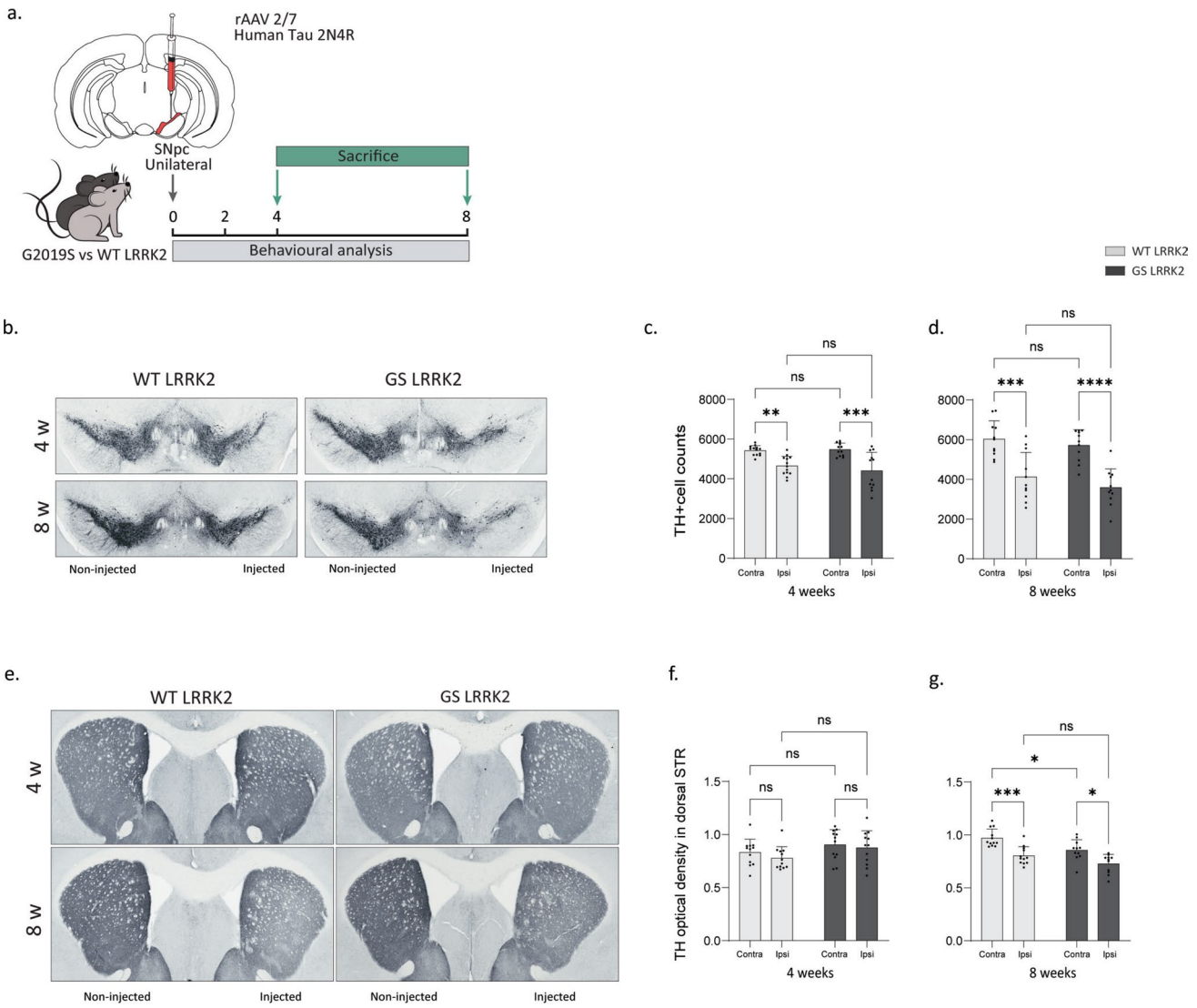

Fig. 5 G2019S LRRK2 mice do not show exacerbated neurodegeneration upon tau overexpression in the SN. **a** Schematic representation of the experimental set up. Mice were unilaterally injected with tau rAAV 2/7 in the SN. **b** Representative images of TH immunostaining in the SN 4 and 8 weeks post-injection of tau rAAV 2/7 in WT and GS LRRK2 mice. **c** Stereological quantification of the TH + cells in the ipsilateral and to the contralateral side 4 and 8 weeks post-injection. **d** Representative images of TH immunostaining in sections from the STR 4 and 8 weeks post-injection of tau rAAV 2/7 in WT and GS LRRK2 mice. **e** Quantification of the TH optical density in the STR at 4 and 8 weeks post-injection in WT and GS LRRK2 mice. N = 12–13 at both the 4 and 8 weeks timepoint. Graphs represent mean ± SD. Statistical differences were assessed using two-way ANOVA followed by Tukey's multiple comparison test. $*p < 0.05$, $**p < 0.01$, $***p < 0.001$, $****p < 0.0001$

that mutant LRRK2 selectively impairs components of the endolysosomal pathway, likely disrupting αSyn clearance via altered vesicle trafficking or autophagosome–lysosome fusion. These observations align with prior studies linking LRRK2 kinase activity to lysosomal dysfunction and αSyn-induced inflammatory signalling [26, 47]. Our findings support a model in which GS LRRK2 exacerbates αSyn toxicity by impairing its degradation and amplifying inflammation, establishing a pathogenic feedback loop.

Although increased cathepsins may stem from immune cell infiltration and activation in GS mice in our model, we cannot exclude neuronal sources. Pathological αSyn can also disrupt neuronal lysosomes, leading to cathepsin release, inflammasome activation, and neuronal death [30]. GS LRRK2 has been shown to disrupt lysosomal morphology, reduce acidification, and impair autophagic flux in neurons, contributing to αSyn accumulation and secretion [73]. Similarly, aged LRRK2 R1441G KI mice exhibit impaired lysosomal degradation, αSyn oligomer build-up, and increased CMA markers like LAMP2A [42]. Since αSyn is mainly degraded via CMA through LAMP2A and cathepsin D, the dysregulation of both in our model indicates that GS LRRK2

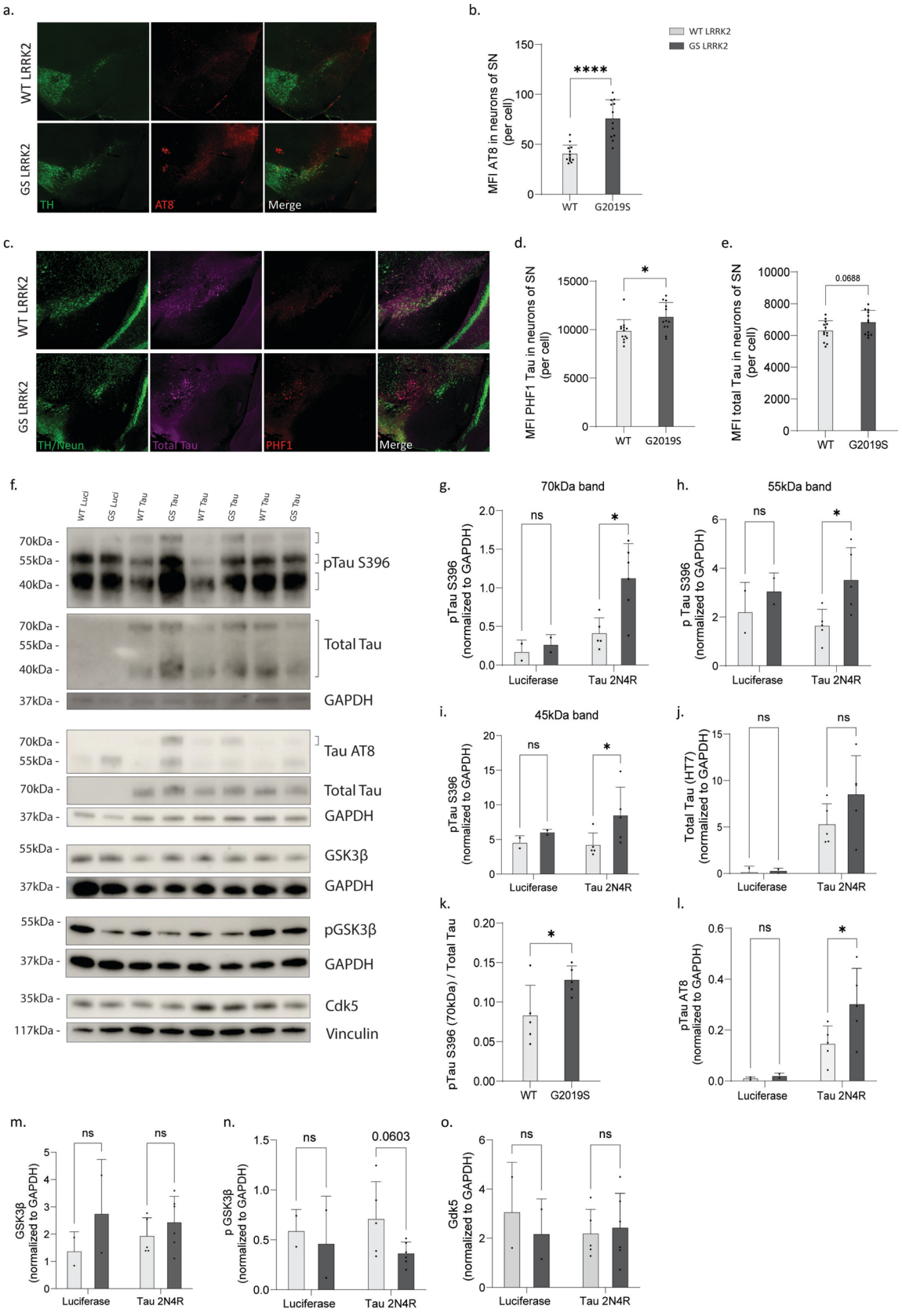
a.
WT LRRK2
GS LRRK2
TH
AT8
Merge
b.
WT LRRK2
GS LRRK2
MFI AT8 in neurons of SN (per cell)
****
WT
G2019S
c.
WT LRRK2
GS LRRK2
TH/Neun
Total Tau
PHF1
Merge
d.
MFI PHF1 Tau in neurons of SN (per cell)
*
WT
G2019S
e.
MFI total Tau in neurons of SN (per cell)
0.0688
WT
G2019S
f.
WT Luci
GS Luci
WT Tau
GS Tau
WT Tau
GS Tau
WT Tau
GS Tau
70kDa -
55kDa -
40kDa -
pTau S396
Total Tau
GAPDH
Tau AT8
GSK3β
pGSK3β
Cdk5
Vinculin
37kDa -
35kDa -
117kDa -
g.
70kDa band
pTau S396 (normalized to GAPDH)
ns
*
Luciferase
Tau 2N4R
h.
55kDa band
p Tau S396 (normalized to GAPDH)
i.
45kDa band
j.
Total Tau (HT7) (normalized to GAPDH)
k.
pTau S396 (70kDa) / Total Tau
l.
pTau AT8 (normalized to GAPDH)
m.
GSK3β (normalized to GAPDH)
n.
p GSK3β (normalized to GAPDH)
0.0603
o.
Gdk5 (normalized to GAPDH)

◂**Fig. 6** G2019S LRRK2 mice show increased tau phosphorylation. **a** Representative images of tau AT8 and TH immunoreactivity in the SN 4 weeks post-injection of tau rAAV 2/7 in WT and GS LRRK2 mice. **b** Quantification of the mean fluorescent intensity of the AT8 + neurons of the SN. **c** Representative immunofluorescent images of total tau, and phosphorylated tau (PHF1) co-stained with TH and NeuN neuronal markers in the SN of tau rAAV 2/7 in WT and GS LRRK2 mice 4 weeks post-injection. Quantification of the mean fluorescent intensity of the PHF1 **d** and total tau **e** signal in neurons of the SN. **f** Western blot analysis of protein extracts from SN of WT and GS LRRK2 mice, 4 weeks after injection with tau rAAV2/7, or controls (fLuc rAAV2/7 or saline). **g**-**n** Densitometric analysis of immunoblots, with signal values normalised to loading controls (GAPDH or vinculin). Blots were probed for pTau S396 (**g**-**i**), pTau AT8 (**l**), total tau (HT7) (**j**), GSK3β (M), pGSK3β S9 (**n**), Cdk5 (**o**). N = 12–13 for immunohistochemistry; n = 4–5 for αSyn rAAV 2/7 groups and $n = 2$ for the control group, for WB analysis. Data are presented as mean ± SD. Statistical analysis was performed using an unpaired Student's t-test. $*p < 0.05$

may compromise CMA and lysosomal proteostasis, promoting αSyn aggregation and toxicity [6, 29]. Furthermore, cathepsin-mediated cell death is a known neurodegenerative mechanism: upon lysosomal membrane permeabilisation, cathepsins B, D, and L can leak into the cytosol, damaging mitochondria and initiating apoptosis or necrosis [2, 59, 61, 76].

Previous studies have reported conflicting findings regarding the role of LRRK2 in tau pathology. Some have suggested that LRRK2 exacerbates tau pathology via direct phosphorylation [9, 46], while others support indirect mechanisms, including altered kinase activity or impaired proteostasis [22, 45, 79]. Although mutant LRRK2 overexpression is reported to increase tau phosphorylation and neuronal toxicity [52], no direct interaction between LRRK2 and tau has been confirmed. In vivo studies using P301S-tau mouse models crossed with GS LRRK2 or LRRK2 KO mice showed minimal effects on tau phosphorylation and aggregation [57, 62], and similar results were obtained when P301S-tau was overexpressed in the hippocampus of these mice. Interestingly, only WT tau overexpression in GS LRRK2 mice led to increased tau propagation [62]. Additional evidence from GS LRRK2 KI mice showed enhanced tau pathology after inoculation with AD-derived tau filaments [16], though no effects were observed in primary neurons exposed to recombinant tau fibrils or AD brain-derived tau [37]. These findings suggest that GS LRRK2 may promote tau transmission rather than tau aggregation per se.

In our study, we build on these observations and show that the GS LRRK2 mutation enhances tau phosphorylation at several epitopes in a 2N4R-tau overexpression model. We use the 2N4R isoform as it robustly undergoes phosphorylation and aggregation in vivo, and is widely used to model tau pathology [82]. Despite this, tau-induced dopaminergic neuron loss, behavioural impairment, and neuroinflammation remained mild and were not significantly altered by the presence of the mutation, indicating a primarily cell-autonomous effect of GS LRRK2 on tau phosphorylation. This is consistent with earlier studies proposing that LRRK2 may influence tau indirectly, particularly through modulation of tau kinases. Prior reports have implicated LRRK2 in regulating GSK-3β activity, one of the key kinases involved in tau phosphorylation, with the GS variant showing stronger binding to GSK-3β [45]. In Drosophila models, LRRK2 overexpression led to increased active (p-Tyr216) GSK-3β levels [49]. In line with this, we observed a strong trend toward decreased levels of the inactive p-Ser9 GSK-3β in the SN of GS mice, without changes in total GSK-3β. This shift toward a more active kinase state could explain the aberrant accumulation of phosphorylated tau. The absence of a clear effect of GS LRRK2 on phospho-tau accumulation in our iPSC-derived dopaminergic neurons may be attributed to the inherently high levels of phospho-tau present in relatively young neurons, or to the limited development of mature tau pathology at the tested time points.

In addition, we did not observe significant alterations in different lysosomal markers in GS LRRK2 mice following tau overexpression, except for a decrease in cathepsin B levels. This finding contrasts with the pronounced lysosomal changes observed in our αSyn overexpression model, suggesting that the impact of the GS mutation on lysosomal pathways varies depending on the pathological trigger. The differential effects of GS LRRK2 on lysosomal function in αSyn versus tau models may reflect differences in how these proteins are processed and degraded, distinct interactions with LRRK2, or divergent associated inflammatory responses. Taken together, our findings align with and expand on previous evidence, indicating that GS LRRK2 promotes tau pathology predominantly via enhanced kinase activity and intracellular phosphorylation rather than through robust effects on inflammation, or neurodegeneration.

A key question in GS LRRK2-linked neurodegeneration is whether immune activation results from impaired protein clearance or is directly driven by the mutation. While αSyn accumulation can trigger inflammation, GS LRRK2 may also intrinsically dysregulate immune responses, promoting chronic neuroinflammation. In our tau model, despite tau accumulation and neuronal loss, no significant immune activation was observed in either WT or GS mice. This suggests that GS LRRK2-mediated immune dysregulation may be specific to αSyn pathology, supporting the idea that neuroinflammation is an early and central event in αSyn-driven disease, worsened by GS LRRK2.

Although our results provide important insights, limitations should be noted. The use of viral overexpression models, while providing control over aggregation timing and localisation, may not fully replicate endogenous disease processes. Moreover, the use of the 2N4R tau isoform may not capture the contribution of 3R tau species also reported

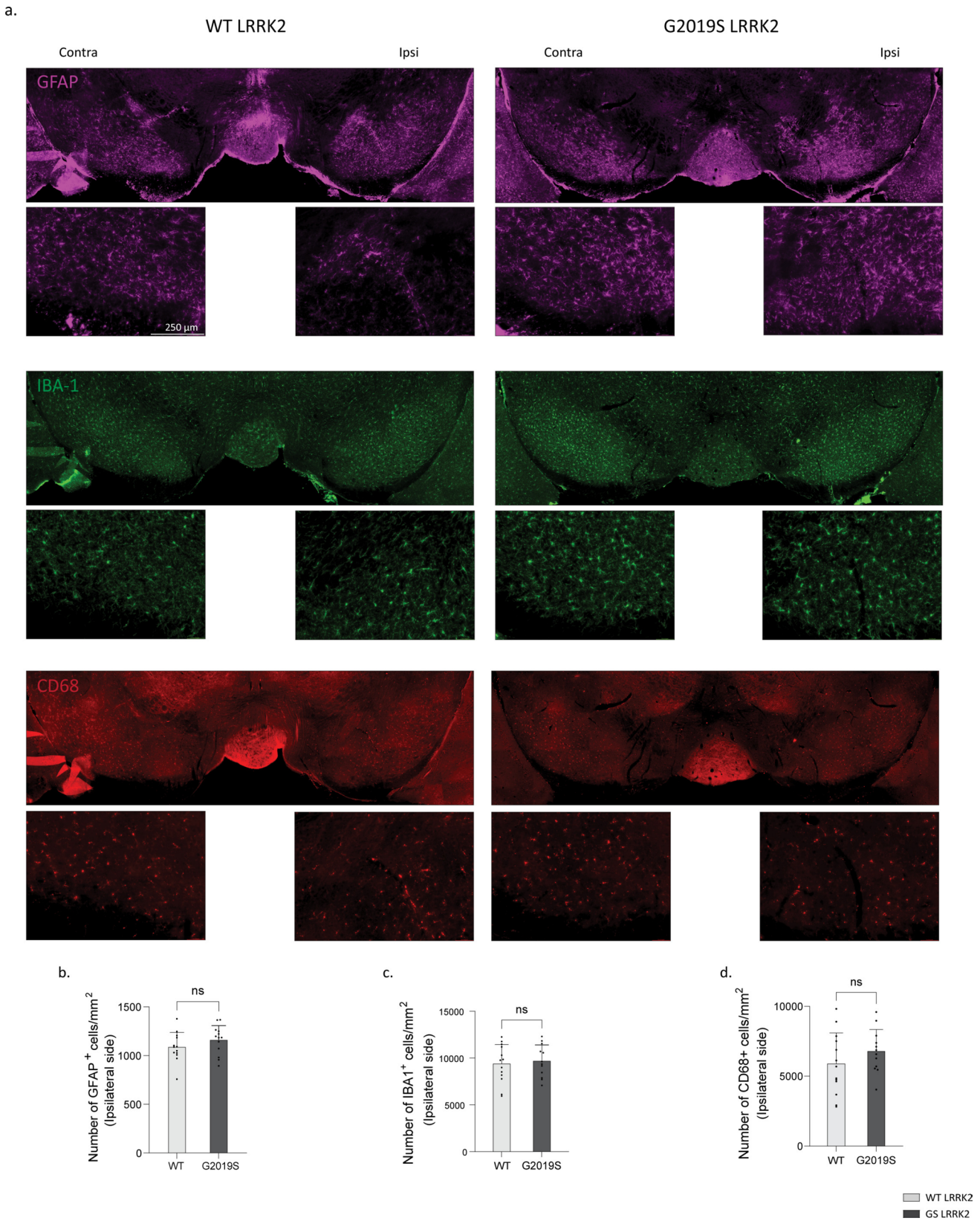

Fig. 7 Inflammatory response is not enhanced in the SN of G2019S mice after tau overexpression. Representative immunofluorescence images of the SN from 4 weeks post-injection of tau rAAV 2/7 in WT and GS LRRK2 mice. **a** Sections were immunostained for astrocytes (GFAP), microglia (IBA1), and activated microglia/macrophages (CD68). Quantification of GFAP$^+$ **b**, IBA1$^+$ **c**, and CD68$^+$ **d** positive cells. N = 12–13 and data are presented as mean ± SD. Statistical analysis was performed using an unpaired Student's t-test

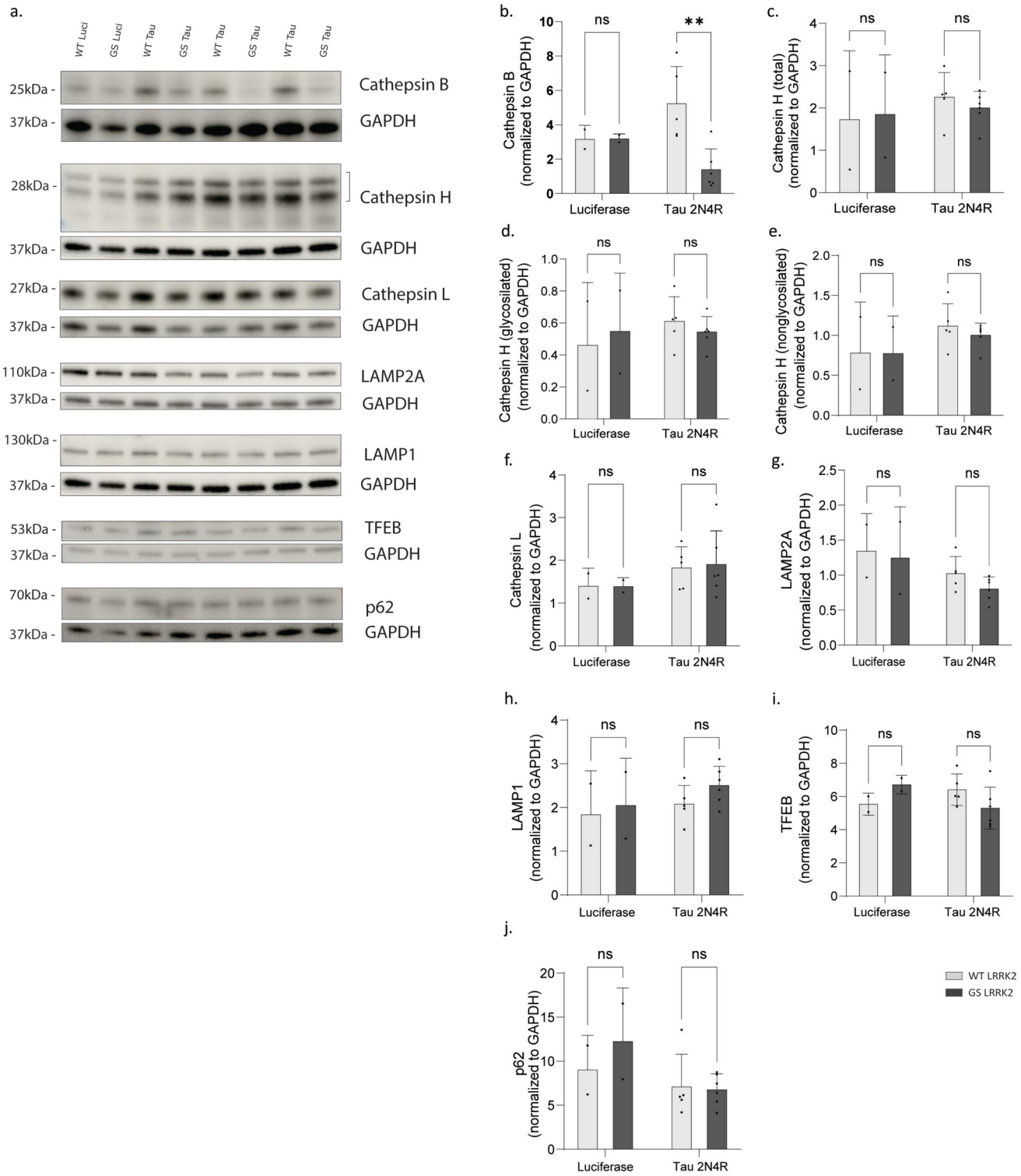

Fig. 8 Characterisation of lysosomal markers in G2019S LRRK2 mice with tau overexpression in SN. Immunoblotting analysis of late endosomal/lysosomal markers in protein extract of SN at 4 weeks after tau- or fLuc-rAAV2/7 injection. **a** Representative western blot images from whole SN protein extracts from WT and GS LRRK2 mice 4 weeks post injection. Immunoblots for Cathepsin B,H,L, Lamp2a, Lamp1, TFEB, and p62 are shown. **b**-**f** Quantification of the protein signal of the blotted proteins. Values were normalised to the endogenous protein (GAPDH) levels. N = 4–5 for αSyn rAAV 2/7 groups and N = 2 for the control group. Graphs represent mean ± SD. Statistical differences were assessed using unpaired Student's t-test. ** $p < 0.01$

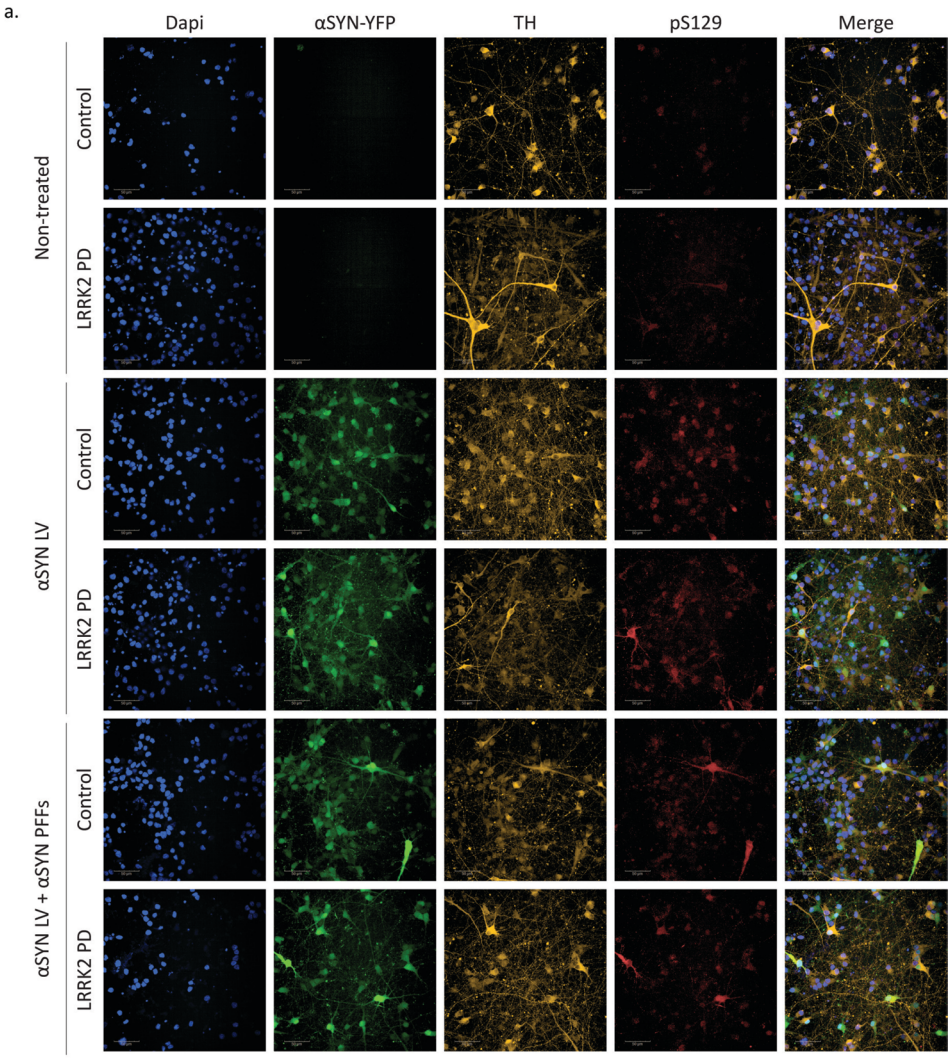

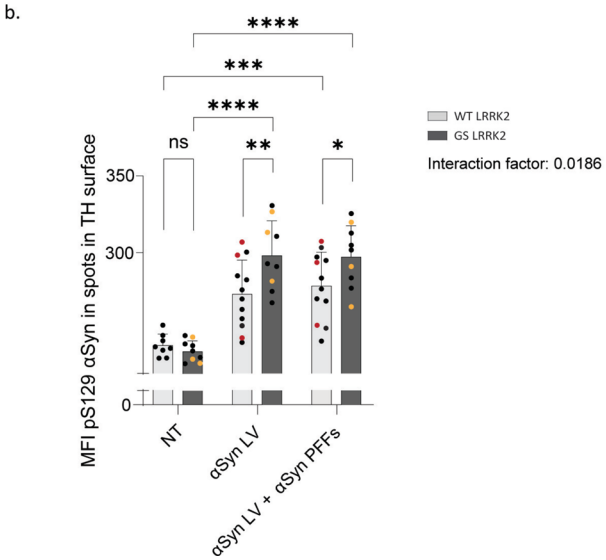

Fig. 9 LRRK2 G2019S increases αSyn phosphorylation in human iPSC-derived dopaminergic neurons. **a** Representative fluorescence images of iPSC lines differentiated to dopaminergic neurons (DIV40) from patients carrying the GS LRRK2 mutation or controls (healthy control and corrected isogenic lines). Three experimental conditions are shown: non-treated cells (NT), cells transduced with αSyn-YFP LV, and cells transduced with αSyn-YFP LV followed by treatment with αSyn PFFs. Immunocytochemistry is shown for TH, pS129 αSyn and αSyn-YFP in neurons transduced with LV to induce overexpression of αSyn-YFP. **b** Quantification of MFI of pS129 αSyn + spots in TH + neurons. Data points represent an iPSC line differentiated to dopaminergic neurons from an independent differentiation. N = 3 iPSC-DaN lines, 3 differentiations. The orange-coloured spot indicates a GS LRRK2 PD line, while the red spot represents its isogenic control. Data are presented as mean ± SD. Statistical analysis was performed using two-way ANOVA followed by Tukey's multiple comparison test. A significant effect was observed for the treatment factor ($p = 0.0186$). *$p < 0.05$, **$p < 0.01$, *** $p < 0.001$, ****$p < 0.0001$

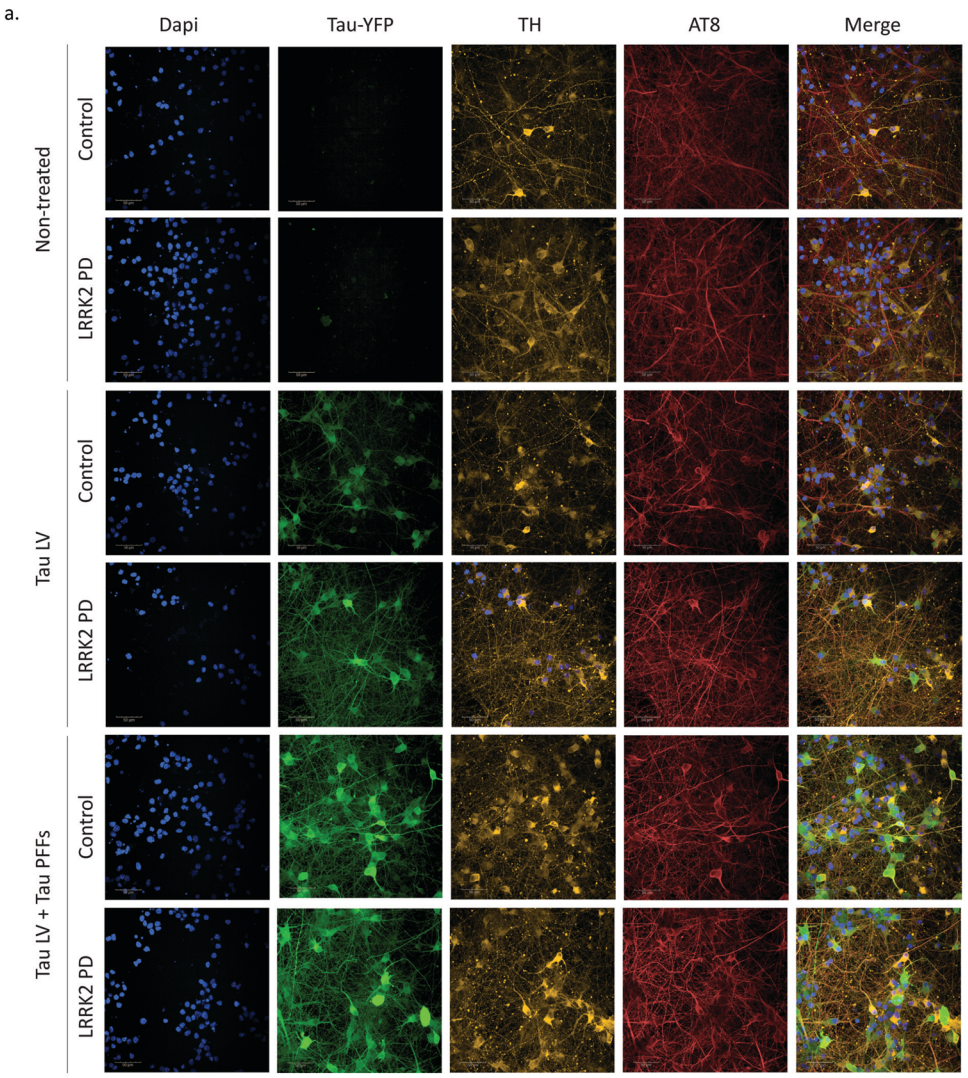

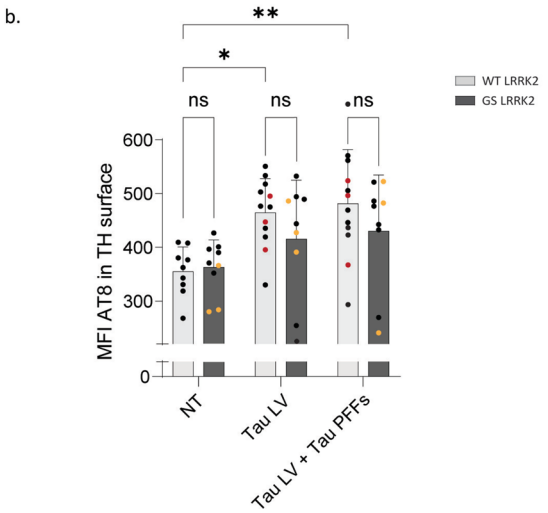

Fig. 10 LRRK2 G2019S does not impact tau phosphorylation in human iPSC-derived dopaminergic neurons. **a** Representative fluorescence images of iPSC lines differentiated to dopaminergic neurons (DIV40) from patients carrying the GS LRRK2 mutation or controls (healthy control and corrected isogenic lines). Three experimental conditions are presented: non-treated cells (NT), cells transduced with tau-YFP LV, and cells transduced with tau-YFP LV and followed by treatment with tau PFFs. Immunocytochemistry for TH, AT8 tau, tau-YFP expressed from the LV transduction. **b** Quantification of MFI of AT8 tau in TH + area. Data points represent an iPSC line differentiated to dopaminergic neurons from an independent differentiation. N = 3 iPSC-DaN lines, 3 differentiations. The orange-coloured spot indicates a GS LRRK2 PD line, while the red spot represents its isogenic control. Data are presented as mean ± SD. Statistical analysis was performed using two-way ANOVA followed by Tukey's multiple comparison test. $^{*}p < 0.05$, $^{**}p < 0.01$

in PD [13]. Further mechanistic studies are needed to dissect the downstream signalling events by which LRRK2 regulates αSyn and tau phosphorylation, immune activation, and lysosomal function. In particular, the precise mechanisms through which LRRK2 influences αSyn pathology, as well as the cell-type origin of the accumulated lysosomal proteins, remain to be elucidated. A major challenge in the field is the complex interplay between α-synuclein and inflammation, and whether they exist in a continuous vicious cycle remains unclear. Future studies will be required to define the exact mechanism by which mutant LRRK2 exacerbates this system. Finally, the findings of our study are also limited to the GS LRRK2 mutant. Given that individual LRRK2 mutations show distinct pathological profiles, such as the I2020T promoting only tau pathology, extrapolation to other variants should be approached with caution.

Conclusion

In conclusion, our results clarify the role of GS LRRK2 in exacerbating αSyn and tau pathology via distinct mechanisms. In the context of αSyn, LRRK2 promotes αSyn neuropathology and neurodegeneration through inflammatory and lysosomal dysregulation. In contrast, its effect on tau appears more directly linked to phosphorylation without triggering secondary inflammatory or lysosomal changes. These findings highlight the mechanistic divergence in how LRRK2 influences key PD-related pathologies and underscore the importance of tailored therapeutic approaches for LRRK2-associated PD. Additionally, these results reinforce the potential of LRRK2 kinase inhibition as a disease-modifying strategy in PD, particularly for mutation carriers, but possibly also for sporadic cases in which LRRK2 activity is elevated.

Supplementary Information The online version contains supplementary material available at https://doi.org/10.1007/s00401-025-02956-6.

Acknowledgements We thank S. Croes, K. Vennekens and Annelies Aertgeerts for their technical assistance; the Leuven Viral Vector Core (LVVC) for the rAAV and LV vector production; and the VIB-KU Leuven FACS and Bioimaging Core Facility.

Author contributions The study was designed and conducted equally by GT and DC. The manuscript was written by GT and DC. LW, IT, EB and MSC assisted with the mouse experiments and corrected the manuscript. CVH was responsible for the rAAV production and transgenic mouse facility. AA supervised the iPSC experiments and corrected the manuscript. RWM supervised the iPSC work and revised the final manuscript. VB coordinated the project and revised the manuscript.

Funding This work was supported by the KU Leuven (C14/18/102), the Michael J Fox Foundation, the Flemish Research Foundation (FWO G0E1917N, SBO S006617N, G031923N, PhD fellowships to GT and DC, and FWO long stay abroad fellowship of GT) and the Queen Elisabeth Medical Foundation. The work in the Wade-Martins Laboratory was funded in part by the Parkinson's UK Monument Discovery Award (J-1403 to RWM) and the MRC Dementia Platform UK Stem Cell Network equipment grant (MC_EX_MR/N50192X/1 to RWM).

Declarations

Ethics approval and consent to participate All animal experiments were carried out in accordance with the European Communities Council Directive of November 24, 1986 (86/609/EEC) and approved by the Bioethical Committee of the KU Leuven (Belgium) (ECD projects 051/2020 and 156/2022). Participants were recruited to the Discovery clinical cohort through the Oxford Parkinson's Disease Center and gave signed informed consent to mutation screening and derivation of iPSC lines from skin biopsies (Ethics committee: National Health Service, Health Research Authority, NRES Committee South Central, Berkshire, UK, REC 10/H0505/71).

Consent for publication The authors consent to the publication. Manuscript was read and approved by all authors.

Data availability All data generated or analyzed during this study is included in this published article [and its supplementary information files].

Competing interests The authors declare that they have no competing interests.

References

1. Aasly JO, Johansen KK, Brønstad G, Warø BJ, Majbour NK, Varghese S et al (2014) Elevated levels of cerebrospinal fluid α-synuclein oligomers in healthy asymptomatic LRRK2 mutation carriers. Front Aging Neurosci. https://doi.org/10.3389/FNAGI.2014.00248
2. Aldini G, Yeum KJ, Russell RM, Krinsky NI (2001) A method to measure the oxidizability of both the aqueous and lipid compartments of plasma. Free Radic Biol Med 31:1043–1050. https://doi.org/10.1016/S0891-5849(01)00684-0
3. Andersen MA, Christensen KV, Badolo L, Smith GP, Jeggo R, Jensen PH et al (2018) Parkinson's disease-like burst firing activity in subthalamic nucleus induced by AAV-α-synuclein is normalized by LRRK2 modulation. Neurobiol Dis 116:13–27. https://doi.org/10.1016/j.nbd.2018.04.011

4. Armstrong GR, Raafat F (1988) Humoral reaction in the inflamed colon in Hirschsprung's disease and ulcerative colitis. J Clin Pathol 41:975–977. https://doi.org/10.1136/JCP.41.9.975
5. Auluck PK, Caraveo G, Lindquist S (2010) α-synuclein: Membrane interactions and toxicity in Parkinson's disease. Annu Rev Cell Dev Biol 26:211–233. https://doi.org/10.1146/ANNUREV.CELLBIO.042308.113313
6. Auzmendi-Iriarte J, Matheu A (2021) Impact of chaperone-mediated autophagy in brain aging: neurodegenerative diseases and glioblastoma. Front Aging Neurosci. https://doi.org/10.3389/FNAGI.2020.630743
7. Bae E-J, Lee S-J (2020) The LRRK2-RAB axis in regulation of vesicle trafficking and α-synuclein propagation. Biochim Biophys Acta Mol Basis Dis 1866:165632. https://doi.org/10.1016/j.bbadis.2019.165632
8. Baekelandt V, Claeys A, Eggermont K, Lauwers E, De Strooper B, Nuttin B et al (2002) Characterization of lentiviral vector-mediated gene transfer in adult mouse brain. Hum Gene Ther 13:841–853. https://doi.org/10.1089/10430340252899019
9. Bailey RM, Covy JP, Melrose HL, Rousseau L, Watkinson R, Knight J et al (2013) LRRK2 phosphorylates novel tau epitopes and promotes tauopathy. Acta Neuropathol 126:809–827. https://doi.org/10.1007/S00401-013-1188-4
10. Balestrino R, Schapira AHV (2020) Parkinson disease. Eur J Neurol 27:27–42. https://doi.org/10.1111/ENE.14108
11. Blauwendraat C, Pletnikova O, Geiger JT, Murphy NA, Abramzon Y, Rudow G et al (2019) Genetic analysis of neurodegenerative diseases in a pathology cohort. Neurobiol Aging 76:214.e1-214.e9. https://doi.org/10.1016/j.neurobiolaging.2018.11.007
12. Cabezudo D, Tsafaras G, Van Acker E, Van den Haute C, Baekelandt V (2023) Mutant LRRK2 exacerbates immune response and neurodegeneration in a chronic model of experimental colitis. Acta Neuropathol 146:245–261. https://doi.org/10.1007/s00401-023-02595-9
13. Chu Y, Hirst WD, Federoff HJ, Harms AS, Stoessl AJ, Kordower JH (2023) Nigrostriatal tau pathology in parkinsonism and Parkinson's disease. Brain 147:444. https://doi.org/10.1093/BRAIN/AWAD388
14. Connor-Robson N, Booth H, Martin JG, Gao B, Li K, Doig N et al (2019) An integrated transcriptomics and proteomics analysis reveals functional endocytic dysregulation caused by mutations in LRRK2. Neurobiol Dis 127:512–526. https://doi.org/10.1016/j.nbd.2019.04.005
15. Cook DA, Kannarkat GT, Cintron AF, Butkovich LM, Fraser KB, Chang J et al (2017) LRRK2 levels in immune cells are increased in Parkinson's disease. NPJ Parkinsons Dis 3:11. https://doi.org/10.1038/s41531-017-0010-8
16. Cornblath EJ, Li HL, Changolkar L, Zhang B, Brown HJ, Gathagan RJ et al (2021) Computational modeling of tau pathology spread reveals patterns of regional vulnerability and the impact of a genetic risk factor. Sci Adv. https://doi.org/10.1126/SCIADV.ABG6677
17. Cremades N, Cohen SIA, Deas E, Abramov AY, Chen AY, Orte A et al (2012) Direct observation of the interconversion of normal and toxic forms of α-synuclein. Cell 149:1048–1059. https://doi.org/10.1016/j.cell.2012.03.037
18. Daher JPL, Abdelmotilib HA, Hu X, Volpicelli-Daley LA, Moehle MS, Fraser KB et al (2015) Leucine-rich repeat kinase 2 (LRRK2) pharmacological inhibition abates α-synuclein gene-induced neurodegeneration. J Biol Chem 290:19433–19444. https://doi.org/10.1074/jbc.M115.660001
19. Daher JPL, Pletnikova O, Biskup S, Musso A, Gellhaar S, Galter D et al (2012) Neurodegenerative phenotypes in an A53T α-synuclein transgenic mouse model are independent of LRRK2. Hum Mol Genet 21:2420–2431. https://doi.org/10.1093/hmg/dds057
20. Daher JPL, Volpicelli-Daley LA, Blackburn JP, Moehle MS, West AB (2014) Abrogation of α-synuclein-mediated dopaminergic neurodegeneration in LRRK2-deficient rats. Proc Natl Acad Sci U S A 111:9289–9294. https://doi.org/10.1073/pnas.1403215111
21. Dinter E, Saridaki T, Nippold M, Plum S, Diederichs L, Komnig D et al (2016) Rab7 induces clearance of α-synuclein aggregates. J Neurochem 138:758–774. https://doi.org/10.1111/JNC.13712
22. Donison N, Hintermayer M, Subramaniam M, Santandrea E, Volkening K, Strong MJ (2023) Upregulation of LRRK2 following traumatic brain injury does not directly phosphorylate Thr175 tau. Front Cell Neurosci. https://doi.org/10.3389/FNCEL.2023.1272899/PDF
23. Dusonchet J, Kochubey O, Stafa K, Young SM, Zufferey R, Moore DJ et al (2011) A rat model of progressive nigral neurodegeneration induced by the Parkinson's disease-associated G2019S mutation in LRRK2. J Neurosci 31:907–912. https://doi.org/10.1523/JNEUROSCI.5092-10.2011
24. Dzamko N, Gysbers AM, Bandopadhyay R, Bolliger MF, Uchino A, Zhao Y et al (2017) LRRK2 levels and phosphorylation in Parkinson's disease brain and cases with restricted Lewy bodies. Mov Disord 32:423–432. https://doi.org/10.1002/mds.26892
25. Dzamko N, Rowe DB, Halliday GM (2016) Increased peripheral inflammation in asymptomatic leucine-rich repeat kinase 2 mutation carriers. Mov Disord 31:889–897. https://doi.org/10.1002/mds.26529
26. Eguchi T, Kuwahara T, Sakurai M, Komori T, Fujimoto T, Ito G et al (2018) LRRK2 and its substrate Rab GTPases are sequentially targeted onto stressed lysosomes and maintain their homeostasis. Proc Natl Acad Sci U S A 115:E9115–E9124. https://doi.org/10.1073/PNAS.1812196115
27. Fantini MC, Dominitzki S, Rizzo A, Neurath MF, Becker C (2007) In vitro generation of cd4+cd25+ regulatory cells from murine naive t cells. Nat Protoc 2:1789–1794. https://doi.org/10.1038/NPROT.2007.258
28. Fearnley JM, Lees AJ (1991) Ageing and Parkinson's disease: substantia nigra regional selectivity. Brain 114(Pt 5):2283–2301. https://doi.org/10.1093/brain/114.5.2283
29. da Fonseca TL, Villar-Piqué A, Outeiro TF (2015) The interplay between alpha-synuclein clearance and spreading. Biomolecules 5:435–471. https://doi.org/10.3390/BIOM5020435
30. Freeman D, Cedillos R, Choyke S, Lukic Z, McGuire K, Marvin S et al (2013) Alpha-synuclein induces lysosomal rupture and cathepsin dependent reactive oxygen species following endocytosis. PLoS One. https://doi.org/10.1371/JOURNAL.PONE.0062143
31. Gardet A, Benita Y, Li C, Sands BE, Ballester I, Stevens C et al (2010) LRRK2 is involved in the IFN-gamma response and host response to pathogens. J Immunol 185:5577–5585. https://doi.org/10.4049/jimmunol.1000548
32. Goedert M, Spillantini MG, Cairns NJ, Crowther RA (1992) Tau proteins of Alzheimer's paired helical filaments: abnormal phosphorylation of all six brain isoforms. Neuron 8:159–168. https://doi.org/10.1016/0896-6273(92)90117-V
33. Greggio E, Jain S, Kingsbury A, Bandopadhyay R, Lewis P, Kaganovich A et al (2006) Kinase activity is required for the toxic effects of mutant LRRK2/dardarin. Neurobiol Dis 23:329–341. https://doi.org/10.1016/j.nbd.2006.04.001
34. Guerreiro PS, Huang Y, Gysbers A, Cheng D, Gai WP, Outeiro TF et al (2013) LRRK2 interactions with α-synuclein in Parkinson's disease brains and in cell models. J Mol Med 91:513–522. https://doi.org/10.1007/S00109-012-0984-Y
35. Gulyás M, Bencsik N, Pusztai S, Liliom H, Schlett K (2016) Animaltracker: an ImageJ-based tracking API to create a customized behaviour analyser program. Neuroinformatics 14:479–481. https://doi.org/10.1007/S12021-016-9303-Z

36. Hakimi M, Selvanantham T, Swinton E, Padmore RF, Tong Y, Kabbach G et al (2011) Parkinson's disease-linked LRRK2 is expressed in circulating and tissue immune cells and upregulated following recognition of microbial structures. J Neural Transm (Vienna) 118:795–808. https://doi.org/10.1007/s00702-011-0653-2
37. Henderson MX, Changolkar L, Trojanowski JQ, Lee VMY (2021) LRRK2 kinase activity does not alter cell-autonomous Tau pathology development in primary neurons. J Parkinsons Dis 11:1187–1196. https://doi.org/10.3233/JPD-212562
38. Henderson MX, Cornblath EJ, Darwich A, Zhang B, Brown H, Gathagan RJ et al (2019) Spread of α-synuclein pathology through the brain connectome is modulated by selective vulnerability and predicted by network analysis. Nat Neurosci 22:1248–1257. https://doi.org/10.1038/s41593-019-0457-5
39. Henderson MX, Sengupta M, McGeary I, Zhang B, Olufemi MF, Brown H et al (2019) LRRK2 inhibition does not impart protection from α-synuclein pathology and neuron death in non-transgenic mice. Acta Neuropathol Commun 7:28. https://doi.org/10.1186/s40478-019-0679-5
40. Henderson MX, Sengupta M, Trojanowski JQ, Lee VMY (2019) Alzheimer's disease tau is a prominent pathology in LRRK2 Parkinson's disease. Acta Neuropathol Commun. https://doi.org/10.1186/S40478-019-0836-X
41. Henry AG, Aghamohammadzadeh S, Samaroo H, Chen Y, Mou K, Needle E et al (2015) Pathogenic LRRK2 mutations, through increased kinase activity, produce enlarged lysosomes with reduced degradative capacity and increase ATP13A2 expression. Hum Mol Genet 24:6013–6028. https://doi.org/10.1093/hmg/ddv314
42. Ho PWL, Leung CT, Liu H, Pang SYY, Lam CSC, Xian J et al (2020) Age-dependent accumulation of oligomeric SNCA/α-synuclein from impaired degradation in mutant LRRK2 knockin mouse model of Parkinson disease: role for therapeutic activation of chaperone-mediated autophagy (CMA). Autophagy 16:347–370. https://doi.org/10.1080/15548627.2019.1603545
43. Jensen NM, Vitic Z, Antorini MR, Bruun Viftrup T, Parkkinen L, Jensen PH (2024) Abundant non-inclusion α-synuclein pathology in Lewy body-negative LRRK2-mutant cases. https://doi.org/10.1101/2024.12.20.629583
44. Kalia LV, Lang AE, Hazrati LN, Fujioka S, Wszolek ZK, Dickson DW et al (2015) Clinical correlations with Lewy body pathology in LRRK2-related Parkinson disease. JAMA Neurol 72:100–105. https://doi.org/10.1001/JAMANEUROL.2014.2704
45. Kawakami F, Shimada N, Ohta E, Kagiya G, Kawashima R, Maekawa T et al (2014) Leucine-rich repeat kinase 2 regulates tau phosphorylation through direct activation of glycogen synthase kinase-3β. FEBS J 281:3–13. https://doi.org/10.1111/FEBS.12579
46. Kawakami F, Yabata T, Ohta E, Maekawa T, Shimada N, Suzuki M et al (2012) LRRK2 phosphorylates tubulin-associated tau but not the free molecule: LRRK2-mediated regulation of the tau-tubulin association and neurite outgrowth. PLoS ONE. https://doi.org/10.1371/JOURNAL.PONE.0030834
47. Kuwahara T, Funakawa K, Komori T, Sakurai M, Yoshii G, Eguchi T et al (2020) Roles of lysosomotropic agents on LRRK2 activation and Rab10 phosphorylation. Neurobiol Dis. https://doi.org/10.1016/j.nbd.2020.105081
48. Lang C, Campbell KR, Ryan BJ, Carling P, Attar M, Vowles J et al (2019) Single-cell sequencing of iPSC-dopamine neurons reconstructs disease progression and identifies HDAC4 as a regulator of Parkinson cell phenotypes. Cell Stem Cell 24:93-106.e6. https://doi.org/10.1016/j.stem.2018.10.023
49. Lin CH, Tsai PI, Wu RM, Chien CT (2010) LRRK2 G2019S mutation induces dendrite degeneration through mislocalization and phosphorylation of tau by recruiting autoactivated GSK3β. J Neurosci 30:13138–13149. https://doi.org/10.1523/JNEUROSCI.1737-10.2010
50. Lin X, Parisiadou L, Gu X-L, Wang L, Shim H, Sun L et al (2009) Leucine-rich repeat kinase 2 regulates the progression of neuropathology induced by Parkinson's-disease-related mutant alpha-synuclein. Neuron 64:807–827. https://doi.org/10.1016/j.neuron.2009.11.006
51. Ling H, Kara E, Bandopadhyay R, Hardy J, Holton J, Xiromerisiou G et al (2013) TDP-43 pathology in a patient carrying G2019S LRRK2mutation and a novel p. Q124E MAPT. Neurobiol Aging 34:2889.e5-2889.e9. https://doi.org/10.1016/j.neurobiolaging.2013.04.011
52. MacLeod D, Dowman J, Hammond R, Leete T, Inoue K, Abeliovich A (2006) The familial Parkinsonism gene LRRK2 regulates neurite process morphology. Neuron 52:587–593. https://doi.org/10.1016/j.neuron.2006.10.008
53. Majbour NK, Aasly JO, Hustad E, Thomas MA, Vaikath NN, Elkum N et al (2020) CSF total and oligomeric α-Synuclein along with TNF-α as risk biomarkers for Parkinson's disease: a study in LRRK2 mutation carriers. Transl Neurodegener. https://doi.org/10.1186/S40035-020-00192-4
54. Manzoni C (2012) LRRK2 and autophagy: a common pathway for disease. Biochem Soc Trans 40:1147–1151. https://doi.org/10.1042/BST20120126
55. Mata I, Salles P, Cornejo-Olivas M, Saffie P, Ross OA, Reed X et al (2023) LRRK2: genetic mechanisms vs genetic subtypes. Handb Clin Neurol 193:133–154. https://doi.org/10.1016/B978-0-323-85555-6.00018-7
56. Meng D, Yang Q, Melick CH, Park BC, Hsieh T-S, Curukovic A et al (2021) Arfgap1 inhibits mTORC1 lysosomal localization and activation. EMBO J 40:e106412. https://doi.org/10.15252/embj.2020106412
57. Mikhail F, Calingasan N, Parolari L, Subramanian A, Yang L, Flint Beal M (2015) Lack of exacerbation of neurodegeneration in a double transgenic mouse model of mutant LRRK2 and tau. Hum Mol Genet 24:3545–3556. https://doi.org/10.1093/HMG/DDV105
58. Mir R, Tonelli F, Lis P, Macartney T, Polinski NK, Martinez TN et al (2018) The Parkinson's disease VPS35[D620N] mutation enhances LRRK2-mediated Rab protein phosphorylation in mouse and human. Biochem J 475:1861–1883. https://doi.org/10.1042/BCJ20180248
59. Mollentze N, Biek R, Streicker DG (2014) The role of viral evolution in rabies host shifts and emergence. Curr Opin Virol 8:68–72. https://doi.org/10.1016/j.coviro.2014.07.004
60. Monfrini E, Di Fonzo A (2017) Leucine-rich repeat kinase (LRRK2) genetics and Parkinson's disease. Adv Neurobiol 14:3–30. https://doi.org/10.1007/978-3-319-49969-7_1
61. Nagelhus EA, Amiry-Moghaddam M, Bergersen LH, Bjaalie JG, Eriksson J, Gundersen V et al (2013) The glia doctrine: addressing the role of glial cells in healthy brain ageing. Mech Ageing Dev 134:449–459. https://doi.org/10.1016/j.mad.2013.10.001
62. Nguyen APT, Daniel G, Valdés P, Islam MS, Schneider BL, Moore DJ (2018) G2019S LRRK2 enhances the neuronal transmission of tau in the mouse brain. Hum Mol Genet 27:120–134. https://doi.org/10.1093/HMG/DDX389
63. Nguyen M, Krainc D (2018) LRRK2 phosphorylation of auxilin mediates synaptic defects in dopaminergic neurons from patients with Parkinson's disease. Proc Natl Acad Sci U S A 115:5576–5581. https://doi.org/10.1073/pnas.1717590115
64. Oliveras-Salvá M, Van Der Perren A, Casadei N, Stroobants S, Nuber S, D'Hooge R et al (2013) RAAV2/7 vector-mediated overexpression of alpha-synuclein in mouse substantia nigra induces protein aggregation and progressive dose-dependent

neurodegeneration. Mol Neurodegener. https://doi.org/10.1186/1750-1326-8-44
65. Orenstein SJ, Kuo S-H, Tasset I, Arias E, Koga H, Fernandez-Carasa I et al (2013) Interplay of LRRK2 with chaperone-mediated autophagy. Nat Neurosci 16:394–406. https://doi.org/10.1038/nn.3350
66. Parisiadou L, Xie C, Cho HJ, Lin X, Gu X-L, Long C-X et al (2009) Phosphorylation of ezrin/radixin/moesin proteins by LRRK2 promotes the rearrangement of actin cytoskeleton in neuronal morphogenesis. J Neurosci 29:13971–13980. https://doi.org/10.1523/JNEUROSCI.3799-09.2009
67. Van der Perren A, Cabezudo D, Gelders G, Peralta Ramos JM, Van den Haute C, Baekelandt V et al (2021) LRRK2 ablation attenuates Alpha-synuclein-induced neuroinflammation without affecting neurodegeneration or neuropathology in vivo. Neurotherapeutics. https://doi.org/10.1007/s13311-021-01007-8
68. Van der Perren A, Toelen J, Casteels C, Macchi F, Van Rompuy A-S, Sarre S et al (2015) Longitudinal follow-up and characterization of a robust rat model for Parkinson's disease based on overexpression of alpha-synuclein with adeno-associated viral vectors. Neurobiol Aging 36:1543–1558. https://doi.org/10.1016/j.neurobiolaging.2014.11.015
69. Poulopoulos M, Levy OA, Alcalay RN (2012) The neuropathology of genetic Parkinson's disease. Mov Disord 27:831–842. https://doi.org/10.1002/MDS.24962
70. Qing H, Wong W, McGeer EG, McGeer PL (2009) Lrrk2 phosphorylates alpha synuclein at serine 129: Parkinson disease implications. Biochem Biophys Res Commun 387:149–152. https://doi.org/10.1016/j.bbrc.2009.06.142
71. Rajput A, Dickson DW, Robinson CA, Ross OA, Dächsel JC, Lincoln SJ et al (2006) Parkinsonism, Lrrk2 G2019S, and tau neuropathology. Neurology 67:1506–1508. https://doi.org/10.1212/01.WNL.0000240220.33950.0C
72. Roosen DA, Cookson MR (2016) LRRK2 at the interface of autophagosomes, endosomes and lysosomes. Mol Neurodegener 11:73. https://doi.org/10.1186/s13024-016-0140-1
73. Schapansky J, Khasnavis S, DeAndrade MP, Nardozzi JD, Falkson SR, Boyd JD et al (2018) Familial knockin mutation of LRRK2 causes lysosomal dysfunction and accumulation of endogenous insoluble α-synuclein in neurons. Neurobiol Dis 111:26–35. https://doi.org/10.1016/j.nbd.2017.12.005
74. Schapansky J, Nardozzi JD, Felizia F, LaVoie MJ (2014) Membrane recruitment of endogenous LRRK2 precedes its potent regulation of autophagy. Hum Mol Genet 23:4201–4214. https://doi.org/10.1093/hmg/ddu138
75. Schildt A, Walker MD, Dinelle K, Miao Q, Schulzer M, O'Kusky J et al (2019) Single inflammatory trigger leads to neuroinflammation in LRRK2 rodent model without degeneration of dopaminergic neurons. J Parkinsons Dis 9:121–139. https://doi.org/10.3233/JPD-181446
76. Schneidman-Duhovny D, Hammel M, Tainer JA, Sali A (2016) FoXS, FoXSDock and MultiFoXS: single-state and multi-state structural modeling of proteins and their complexes based on SAXS profiles. Nucleic Acids Res 44:W424–W429. https://doi.org/10.1093/NAR/GKW389
77. Sekiya H, Franke L, Hashimoto Y, Takata M, Nishida K, Futamura N et al (2025) Widespread distribution of α-synuclein oligomers in LRRK2-related Parkinson's disease. Acta Neuropathol 149:42. https://doi.org/10.1007/S00401-025-02872-9
78. Shahmoradian SH, Lewis AJ, Genoud C, Hench J, Moors TE, Navarro PP, Castaño-Díez D, Schweighauser G, Graff-Meyer A, Goldie KN, Sütterlin R, Huisman E, Ingrassia A, Gier Y de, Rozemuller AJM, Wang J, Paepe A De, Erny J, Staempfli A, Hoernschemeyer J, Großerüschkamp F, Niedieker D, El-Mashtoly SF, Quadri M, Van Ijcken WFJ, Bonifati V, Gerwert K, Bohrmann B, Frank S, Britschgi M, Stahlberg H, Van de Berg WDJ, Lauer ME (2019) Lewy pathology in Parkinson's disease consists of crowded organelles and lipid membranes. Nat Neurosci 22:1099–1109. https://doi.org/10.1038/S41593-019-0423-2
79. Shanley MR, Hawley D, Leung S, Zaidi NF, Dave R, Schlosser KA et al (2015) LRRK2 facilitates tau phosphorylation through strong interaction with tau and cdk5. Biochemistry 54:5198–5208. https://doi.org/10.1021/ACS.BIOCHEM.5B00326
80. Siderowf A, Concha-Marambio L, Lafontant DE, Farris CM, Ma Y, Urenia PA et al (2023) Assessment of heterogeneity among participants in the Parkinson's progression markers initiative cohort using α-synuclein seed amplification: a cross-sectional study. Lancet Neurol 22:407–417. https://doi.org/10.1016/S1474-4422(23)00109-6
81. Singh A, Zhi L, Zhang H (2019) LRRK2 and mitochondria: recent advances and current views. Brain Res 1702:96–104. https://doi.org/10.1016/j.brainres.2018.06.010
82. Sinnige T, Stroobants K, Dobson CM, Vendruscolo M (2020) Biophysical studies of protein misfolding and aggregation in in vivo models of Alzheimer's and Parkinson's diseases. Q Rev Biophys 53:e10. https://doi.org/10.1017/S0033583520000025
83. Spillantini MG, Crowther RA, Jakes R, Hasegawa M, Goedert M (1998) Alpha-synuclein in filamentous inclusions of Lewy bodies from Parkinson's disease and dementia with Lewy bodies. Proc Natl Acad Sci U S A 95:6469–6473. https://doi.org/10.1073/pnas.95.11.6469
84. Stafa K, Trancikova A, Webber PJ, Glauser L, West AB, Moore DJ (2012) GTPase activity and neuronal toxicity of Parkinson's disease-associated LRRK2 is regulated by ArfGAP1. PLoS Genet 8:e1002526. https://doi.org/10.1371/journal.pgen.1002526
85. Steger M, Tonelli F, Ito G, Davies P, Trost M, Vetter M et al (2016) Phosphoproteomics reveals that Parkinson's disease kinase LRRK2 regulates a subset of Rab GTPases. Elife. https://doi.org/10.7554/eLife.12813
86. Thévenet J, Pescini Gobert R, Hooft van Huijsduijnen R, Wiessner C, Sagot YJ (2011) Regulation of LRRK2 expression points to a functional role in human monocyte maturation. PLoS ONE 6:e21519. https://doi.org/10.1371/journal.pone.0021519
87. Volles MJ, Lansbury PT (2003) Zeroing in on the pathogenic form of α-synuclein and its mechanism of neurotoxicity in Parkinson's disease. Biochemistry 42:7871–7878. https://doi.org/10.1021/BI030086J
88. Volpicelli-Daley LA, Abdelmotilib H, Liu Z, Stoyka L, Daher JPL, Milnerwood AJ et al (2016) G2019S-LRRK2 expression augments α-synuclein sequestration into inclusions in neurons. J Neurosci 36:7415–7427. https://doi.org/10.1523/JNEUROSCI.3642-15.2016
89. Wakabayashi K, Tanji K, Odagiri S, Miki Y, Mori F, Takahashi H (2013) The Lewy body in Parkinson's disease and related neurodegenerative disorders. Mol Neurobiol 47:495–508. https://doi.org/10.1007/S12035-012-8280-Y
90. Wauters F, Cornelissen T, Imberechts D, Martin S, Koentjoro B, Sue C et al (2020) *LRRK2* mutations impair depolarization-induced mitophagy through inhibition of mitochondrial accumulation of *RAB10*. Autophagy 16:203–222. https://doi.org/10.1080/15548627.2019.1603548
91. Williamson MG, Madureira M, McGuinness W, Heon-Roberts R, Mock ED, Naidoo K et al (2023) Mitochondrial dysfunction and mitophagy defects in *LRRK2-R1441C* Parkinson's disease models. Hum Mol Genet 32:2808–2821. https://doi.org/10.1093/hmg/ddad102
92. Winner B, Jappelli R, Maji SK, Desplats PA, Boyer L, Aigner S et al (2011) In vivo demonstration that α-synuclein oligomers are toxic. Proc Natl Acad Sci U S A 108:4194–4199. https://doi.org/10.1073/PNAS.1100976108/-/DCSUPPLEMENTAL/PNAS.201100976SI.PDF

93. Ysselstein D, Nguyen M, Young TJ, Severino A, Schwake M, Merchant K et al (2019) LRRK2 kinase activity regulates lysosomal glucocerebrosidase in neurons derived from Parkinson's disease patients. Nat Commun. https://doi.org/10.1038/S41467-019-13413-W
94. Zambon F, Cherubini M, Fernandes HJR, Lang C, Ryan BJ, Volpato V et al (2019) Cellular α-synuclein pathology is associated with bioenergetic dysfunction in Parkinson's *i*PSC-derived dopamine neurons. Hum Mol Genet 28:2001–2013. https://doi.org/10.1093/hmg/ddz038
95. Zhang X, Gao F, Wang D, Li C, Fu Y, He W et al (2018) Tau pathology in Parkinson's disease. Front Neurol 9:809. https://doi.org/10.3389/FNEUR.2018.00809
96. Zhao HT, John N, Delic V, Ikeda-Lee K, Kim A, Weihofen A et al (2021) Erratum: LRRK2 antisense oligonucleotides ameliorate α-synuclein inclusion formation in a Parkinson's disease mouse model. Mol Ther Nucleic Acids 25:152–154
97. Zimprich A, Biskup S, Leitner P, Lichtner P, Farrer M, Lincoln S et al (2004) Mutations in LRRK2 cause autosomal-dominant parkinsonism with pleomorphic pathology. Neuron 44:601–607. https://doi.org/10.1016/j.neuron.2004.11.005